

## The Estimation of Snowfall Rate Using Visibility

ROY M. RASMUSSEN, JOTHIRAM VIVEKANANDAN, AND JEFFREY COLE

*National Center for Atmospheric Research, Boulder, Colorado*

BARRY MYERS

*Transport Canada, Montreal, Quebec, Canada*

CHARLES MASTERS

*Federal Aviation Administration Hughes Technical Center, Atlantic City, New Jersey*

(Manuscript received 17 February 1998, in final form 29 September 1998)

### ABSTRACT

The relationship between liquid equivalent snowfall rate and visibility is investigated using data collected at the National Center for Atmospheric Research Marshall Snowfall Test Site during two winter field seasons and using theoretical relationships. The observational data include simultaneous liquid equivalent snowfall rate, crystal types, and both automated and manual visibility measurements. Theoretical relationships between liquid equivalent snowfall rate and visibility are derived for 27 crystal types, and for “dry” and “wet” aggregated snowflakes. Both the observations and theory show that the relationship between liquid equivalent snowfall rate and visibility depends on the crystal type, the degree of riming, the degree of aggregation, and the degree of wetness of the crystals, leading to a large variation in the relationship between visibility and snowfall rate. Typical variations in visibility for a given liquid equivalent snowfall rate ranged from a factor of 3 to a factor of 10, depending on the storm. This relationship is shown to have a wide degree of scatter from storm to storm and also during a given storm. The main cause for this scatter is the large variation in cross-sectional area to mass ratio and terminal velocity for natural snow particles.

It also is shown that the visibility at night can be over a factor of 2 greater than the visibility during the day for the same atmospheric extinction coefficient. Since snowfall intensity is defined by the U.S. National Weather Service using visibility, this day/night difference in visibility results in a change in snowfall intensity category caused by only whether it is day or night. For instance, a moderate snowfall intensity during the day will change to a light snowfall intensity at night, and a heavy snowfall intensity during the day will change to a moderate snowfall intensity at night, for the same atmospheric extinction coefficient.

Thus, the standard relationship between snowfall intensity and visibility used by many national weather services (1/4 mile or less visibility corresponds to heavy snowfall intensity, between 5/16 and 5/8 mile corresponds to moderate intensity, and greater than 5/8 mile corresponds to light intensity) does not always provide the correct indication of actual liquid equivalent snowfall rate because of the variations in snow type and the differences in the nature of visibility targets during day and night. This false indication may have been a factor in previous ground-deicing accidents in which light snow intensity was reported based on visibility, when in fact the actual measured liquid equivalent snowfall rate was moderate to heavy.

### 1. Introduction

Current methods of estimating snowfall intensity operationally in the United States and Canada are based either entirely or partially on prevailing visibility.<sup>1</sup> The

U.S. National Weather Service manual (nonautomatic) estimates of snow intensity are determined by either transmissometer estimates of visibility or by an observer sighting on objects a known distance away. Light snow intensity (−SN) is reported when the visibility is greater than or equal to 5/8 mi (1.0 km), moderate snow intensity (SN) is reported when the visibility is less than 5/8 mi but greater than 1/4 mi (0.5 km), and heavy snow intensity (+SN) occurs when the visibility is less than or equal to 1/4 mi (National Weather Service 1994). Automatic snowfall intensity measurements from the Automated Surface Observing System (ASOS) are determined using a Light Emitting Diode Weather Indicator (LEDWI) system that automatically determines

<sup>1</sup> Prevailing visibility is the greatest horizontal visibility that is equaled or surpassed throughout half of the horizon circle (it need not be a continuous half).

*Corresponding author address:* Dr. Roy M. Rasmussen, NCAR, Research Applications Program, 3450 Mitchell Ln., Bldg. 2, P.O. Box 3000, Boulder, CO 80307-3000.  
E-mail: rasmus@ucar.edu

whether the precipitation type is snow or rain by using the scintillation pattern produced by precipitation as it falls through a collimated infrared beam. Snow intensity is determined by the 1-min sum of low-frequency amplitude modulations due to snow. These snow intensities are adjusted, however, to be compatible with the visibility measured by the ASOS forward scatter visibility sensor (Belfort 6220) according to the following rules.

- 1) If the LEDWI estimated intensity is light (-SN), no change is made.
- 2) If the LEDWI intensity is moderate (SN) or heavy (+SN) and the Belfort visibility is greater than 3/4 mi, the snowfall intensity is changed to light (-SN).
- 3) If the LEDWI intensity is heavy (+SN) and the Belfort visibility is greater than or equal to 1/2 mi, the intensity is changed to moderate (SN).

Since the output of the ASOS visibility instrument is in 1/4-mi increments for visibilities less than 2 mi, the snowfall intensity is defined as heavy for visibilities of 1/4 mi or less, moderate for 1/2-mi visibility, and light for visibilities of 3/4 mi or greater (National Weather Service 1994). Thus, both manual and automatic methods of estimating current snowfall intensity are based either entirely or partially on the visibility during a snow event. These estimates are reported hourly by the U.S. National Weather Service in Aviation Routine Weather Report [METAR (Fr)] reports or more frequently if conditions are changing.

Recent analysis of aircraft accidents caused by snow or ice on an aircraft's wing during takeoff (Rasmussen et al. 1995) has suggested that visibility may not provide estimates of snowfall intensity that are sufficiently accurate for airline use during ground-deicing operations. Many of the major ground-deicing accidents had similar meteorological conditions of temperature, wind speed, and liquid equivalent snowfall rate<sup>2</sup> but widely varying visibilities (Table 1 and Rasmussen et al. 1995). Since snowfall intensity is estimated using visibility as mentioned above, the snowfall intensity information that was available to the pilots during these accidents also varied widely, ranging from light to nearly heavy snowfall intensity despite the nearly constant liquid equivalent snowfall rate as determined from National Weather Service weighing snow gauges (recorded hourly but reported every 3 h). The liquid equivalent snowfall rate from National Weather Service weighing snow gauges for the five deicing accidents investigated by Rasmussen et al. (1995) (Table 1) ranged from only 2.0 to 2.5 mm h<sup>-1</sup>, while the visibility ranged from 0.38 to 3.0 km. Of particular interest is the La Guardia accident, which was associated with a light snowfall intensity (according to the visibility criterion) and wet snow conditions prior

<sup>2</sup> Liquid equivalent snowfall rate is defined as the amount of melted snowfall per unit time and is typically measured by a snow gauge in mm h<sup>-1</sup>.

TABLE 1. U.S. jet transport takeoff icing accidents in snow conditions.

Accident location	Date	Accident time (UTC)	Type of aircraft	Precipitation rate (mm h <sup>-1</sup> ), obs period (UTC)	Precipitation type	Visibility (mi), UTC time	Wind speed (kt), wind direction	Temperature	Wet-bulb temperature
Newark, NJ (Newark International)	27 Nov 1978	1650	DC-9	2.13, 1600-1700	Light snow and fog	0.50, 1600	8, 30°	27°F (-2.8°C)	27°F (-2.8°C)
Boston, MA (Logan International)	16 Feb 1980	1908	BB-253F	2.0, 1800-1900	Light snow and fog	2.0, 1854	11, 330°	30°F (-1.1°C)	28°F (-2.2°C)
Washington, DC (National)	13 Jan 1982	2100	B-737	2.25, 2000-2100	Moderate snow	0.38, 2000	8, 20°	25°F (-3.9°C)	25°F (-3.9°C)
Denver, CO (Stapleton)	15 Nov 1987	2115	DC-9	2.5, 2100-2200	Moderate snow	0.5, 2100	10, 30°	27°F (-2.8°C)	27°F (-2.8°C)
Flushing, NY (La Guardia)	23 Mar 1992	0235	F-28	2.5, 0200-0240	Light snow	0.75, 0200	13, 70°	31°F (-0.6°C)	30.5°F (-0.85°C)

to the accident (as reported by the National Weather Service observer and consistent with the relatively warm wet-bulb temperature of 30.5°F; see Table 1). This case occurred at night—a condition that will be shown to cause an increase in visibility.

To determine the conditions under which high visibility and high liquid equivalent snowfall rates can occur, the National Center for Atmospheric Research (NCAR) Marshall field site, located 5 miles south of Boulder, Colorado, was instrumented with a variety of weighing snow gauges and automatic visibility sensors and simultaneous visibility and liquid equivalent snowfall data collected during the winters of 1994/95 and 1995/96. This paper presents an analysis of these data in section 3. New theoretical relationships between liquid equivalent snowfall rate and visibility for dry snow, wet snow, and 27 different ice crystal types are presented in section 4.

A discussion of the water content of single ice crystals and snowflakes is presented in section 2 to provide background information on the discussion to follow. Comparison of the observations at Marshall to the current theoretical results is made in section 5. Section 6 discusses the effect of nightfall on snow intensity defined by visibility. In section 7, concluding remarks are given. To simplify notation, the term “snowfall rate” will refer to liquid equivalent snowfall rate, and “snowfall intensity” will refer to light, moderate, and heavy snowfall intensities as estimated by visibility. Light, moderate, and heavy liquid equivalent snowfall rates in this paper are defined as 0–1.0 mm h<sup>-1</sup>, 1.0–2.5 mm h<sup>-1</sup>, and greater than 2.5 mm h<sup>-1</sup>, respectively, consistent with the usage by the Society of Automotive Engineers to characterize snowfall rates for deicing fluids.

## 2. Background: Water content of ice crystals and snowflakes

### a. Water content of single ice crystals

Most single ice crystals have a bulk density that is less than that of bulk ice. This fact most often is caused by the skeletal growth pattern of ice crystals, which often creates hollow regions in the interior of the crystals (e.g., hollow columns). The water content, or density, of single crystals has been studied by a number of investigators (Ono 1969; Heymsfield 1972; Iwai 1973; Jayaweera and Ohtake 1974; Heymsfield and Kajikawa 1987; Zikmumda and Vali 1972; Mitchell et al. 1990). Table 2 summarizes ice crystal properties, including bulk densities as given by Heymsfield and Kajikawa (1987) for platelike crystals and by Heymsfield (1972) for columnar-type crystals. The bulk density of a plate-like crystal is calculated by assuming that the bulk volume is given by the maximum diameter and thickness of the crystal. Thus, the density of a dendritic crystal is given as 0.5 g cm<sup>-3</sup>, much less than that of solid ice. For the most part, ice crystal densities are greater than

0.5 g cm<sup>-3</sup>, reflecting the fact that ice crystals are mostly pure ice of density 0.9 g cm<sup>-3</sup>. Also note that the bulk ice crystal densities for the 27 listed crystal types typically have a standard deviation of only ±10% of the average value.

### b. Water content of snowflakes (particles consisting of two or more single ice crystals)

In contrast to the relatively small variation in ice crystal density, snowflake density has been shown to vary over two orders of magnitude, from 0.005 to 0.2 g cm<sup>-3</sup>, with the largest flakes having the lowest density (Magono and Nakamura 1965). If the component ice crystals of a snowflake were as closely packed as possible, the density of the snowflake should be 0.75 times the density of the component crystals (Conway and Sloane 1993). As mentioned above, the component crystal density is typically 0.5 g cm<sup>-3</sup> or greater; thus the aggregate density in this case would be 0.38 g cm<sup>-3</sup>. The extremely low densities observed in natural snow suggest that ice crystals in snowflakes are very loosely packed, with the closeness of the packing decreasing with increasing snowflake size. This relationship between snowflake density and snowflake diameter has been studied by Magono and Nakamura (1965) and by Rogers (1974). Holroyd (1971), using data from Magono and Nakamura (1965), showed that dry snowflake density is inversely proportional to snowflake diameter  $D$  and equal to  $\rho_{s,dry} = 0.017D^{-1}$  (Fig. 1). For wet and/or rimed snowflakes, Rogers (1974) showed that the inverse relationship between snowflake density and size still held, but that the constant of proportionality was equal to 0.0724 g cm<sup>-2</sup>, over four times larger than the dry snow case (Fig. 1):  $\rho_{s,wet} = 0.0724D^{-1}$ . As will be shown later, this relation results in a factor of 4 increase in visibility for wet or rimed snow as compared to dry snow for a given liquid equivalent snowfall rate. Visibility is increased also by the higher terminal velocity of wet or rimed snow as compared to dry snow (typically a factor of 2, from 1 to 2 m s<sup>-1</sup>). This effect increases visibility for a given liquid equivalent snowfall rate by a factor of 2. Thus, the net effect on visibility of wet or rimed snow is predicted to be an increase of over a factor of 8.

The nearly constant fall velocity of snowflakes is a direct result of the density being inversely proportional to the snowflake diameter. For a spherical snowflake of density  $\rho_s$ , the terminal velocity can be written as (Pruppacher and Klett 1997)

$$V_t = \left( \frac{4g\rho_s D}{3C_D\rho_a} \right)^{1/2}, \quad (1)$$

where  $C_D$  is the drag coefficient for snow,  $g$  is the acceleration of gravity, and  $\rho_a$  is the density of air. The drag coefficient for dry snow was determined by Magono and Nakamura (1965) to be nearly constant at a value of 1.3. If the snowflake density in the above equa-

TABLE 2. Ice crystal and snowflake cross-sectional area, volume, density, terminal velocity, and mass at 1000 mb; diameter  $D$  in cm or length  $L$  in cm. Information from Heymsfield and Kajikawa (1987), Heymsfield (1972), Mitchell et al. (1989), Jayaweera and Cottis (1968), Jayaweera and Ohtake (1974), Inai (1973), Zikmunda and Vali (1972), and Davis (1974).

Habit designation	Crystal type		Edge-on			Density		Terminal			$r^2$		
	Habit description	cross-sectional area (cm <sup>2</sup> ) = $A_s = aD^b$	$a$	$b$	Volume (cm <sup>3</sup> ) = $V = cD^d$	(g cm <sup>-3</sup> ) = $\rho_s = eD^f$ (mean, $\pm 1\sigma$ )	$e$	$f$	velocity = $V_t = gD^h$	$g$		$h$	$m-D$ relation
C1h	Thick plate	0.0359	1.68	0.0282	2.68	0.93 $\pm$ 0.10	-0-	1457	1.09	2.63 $\times 10^{-2}D^{0.68}$	0.67		
P1a	Hexagonal plate	0.0531	2.31	0.0417	3.31	0.90 $\pm$ 0.15	-0-	297	0.86	3.76 $\times 10^{-2}D^{0.31}$	0.93		
P1b	w/sectorlike branches	0.0097	1.83	0.00764	2.83	0.83 $\pm$ 0.10	-0-	190	0.81	6.34 $\times 10^{-3}D^{0.83}$	0.97		
P1c	w/broad branches	0.00795	1.79	0.00625	2.79	0.60 $\pm$ 0.11	-0-	103	0.62	3.76 $\times 10^{-3}D^{0.79}$	0.96		
P1d	Stellar	0.0027	1.59	0.0022	2.59	0.44 $\pm$ 0.08	-0-	58	0.55	9.61 $\times 10^{-4}D^{0.59}$	0.95		
P1e	Dendrite	0.0015	1.29	0.0012	2.29	0.50 $\pm$ 0.09	-0-	55	0.48	6.12 $\times 10^{-4}D^{0.29}$	0.98		
P2a	Stellar w/end plates	0.00447	1.53	0.0036	2.53	0.60 $\pm$ 0.11	-0-	72	0.33	2.11 $\times 10^{-3}D^{0.33}$	0.88		
P2c	Dendrite w/end plates	0.00614	2.12	0.005	3.12	0.55 $\pm$ 0.10	-0-	54	0.20	2.66 $\times 10^{-3}D^{0.12}$	0.76		
P2e	Plate w/extensions	0.0085	1.81	0.0066	2.81	0.64 $\pm$ 0.11	-0-	129	0.68	4.29 $\times 10^{-3}D^{0.81}$	0.95		
P2g	Plate w/dendritic extensions	0.0094	1.94	0.0073	2.94	0.63 $\pm$ 0.10	-0-	160	0.80	4.68 $\times 10^{-3}D^{0.94}$	0.97		
P6c	Stellar w/spatial plates	0.0014	1.02	0.0011	2.02	0.54 $\pm$ 0.08	-0-	57	0.21	6.20 $\times 10^{-4}D^{0.02}$	0.77		
P6d	Stellar w/spatial dendrites	0.00217	1.55	0.0017	2.55	0.54 $\pm$ 0.07	-0-	60	0.37	9.23 $\times 10^{-4}D^{0.55}$	0.93		
P7a	Radiating assemblages of plates	0.00354	0.80	0.0028	1.8	0.52 $\pm$ 0.03	-0-	60	0.37	1.45 $\times 10^{-3}D^{1.8}$			
P7b	Radiating assemblages of dendrites	0.00396	1.68	0.0031	2.68	0.49 $\pm$ 0.08	-0-	137	0.83	1.53 $\times 10^{-3}D^{0.68}$	0.91		
R1c	Rimed plates	0.00668	1.36	0.0053	2.36	0.80 $\pm$ 0.18	-0-	92	0.27	4.21 $\times 10^{-3}D^{0.36}$	0.85		
R1d	Rimed stellar	0.00416	1.58	0.0034	2.58	0.62 $\pm$ 0.10	-0-	79	0.36	2.03 $\times 10^{-3}D^{0.58}$	0.85		
R2a	Densely rimed plate	0.15	2.8	0.12	3.8	0.81 $\pm$ 0.17	-0-	92	0.07	9.53 $\times 10^{-2}D^{0.80}$	0.46		
R2b	Densely rimed stellar	0.015	2.04	0.012	3.04	0.64 $\pm$ 0.10	-0-	162	0.53	7.55 $\times 10^{-3}D^{0.04}$	0.78		
R2c	Stellar w/rimed spatial branches	0.0015	0.74	0.0012	1.74	0.61 $\pm$ 0.12	-0-	75	0.24	7.25 $\times 10^{-4}D^{1.74}$	0.69		
R3b	Heavily rimed dendrites	0.003	0.7	0.0023	1.7	0.58 $\pm$ 0.11	-0-	162	0.53	1.35 $\times 10^{-3}D^{1.7}$	0.89		
R4b	Lump graupel	0.78	2.0	0.52	3.0	0.3	-0-	733	0.89	1.07 $\times 10^{-1}D^{0.10}$	0.95		
R4c	Conical graupel	0.78	2.0	0.52	3.0	0.3	-0-	590	0.76	7.61 $\times 10^{-2}D^{0.38}$	0.94		
C1e	Short columns	0.21	1.8	0.0357	2.6	0.7	-0-	1500	1.09	9.42 $\times 10^{-2}D^{0.06}$	0.92		
N1e	Long columns	3.72	1.4	0.108	1.8	0.7	-0-	757	0.80	1.76 $\times 10^{-1}D^{0.06}$	0.97		
N1a	Elementary needles	0.022	1.4	0.00038	1.8	0.8	-0-	104	0.80	5.74 $\times 10^{-2}D^{0.88}$	0.96		
R1a	Rimed elementary needle	0.04	1.55	0.00125	2.1	0.6	-0-	208	0.80	2.5 $\times 10^{-2}L^{2.6}$			
R1b	Rimed long columns	0.06	1.4	0.0029	1.8	0.5	-0-	1500	0.80	7.6 $\times 10^{-2}L^{1.8}$			
Dry unrimed spherical snowflake		$\pi/4$	2.0	$\pi/6$	3.0	0.017	-1	107	0.2	3.1 $\times 10^{-4}L^{1.8}$			
Wet or rimed spherical snowflake		$\pi/4$	2.0	$\pi/6$	3.0	0.072	-1	214	0.2	7.5 $\times 10^{-4}L^{2.1}$			

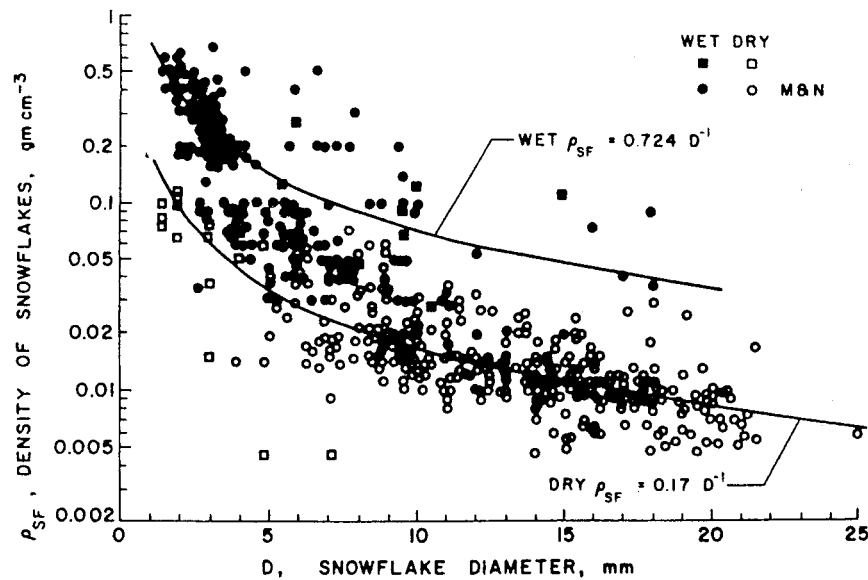


FIG. 1. Average snowflake density versus snowflake diameter from Magono and Nakamura (1965), represented as open and solid-filled circles, and from Rogers (1974), represented as open and solid-filled squares. The curve for the dry snowflakes represents the least squares equation from Holroyd (1971) and the curve for wet snowflakes represents the least squares curve from Rogers (1974). [From Rogers (1974).]

tion were constant for all sizes, the snowflake terminal velocity would increase as the square root of diameter. Observations by Magono and Nakamura (1965) and others, however, have shown that the terminal velocity of dry and wet or rimed snowflakes is nearly constant with size. In order for this observation to be true, then the quantity  $\rho_s D$  has to be a constant as discussed above. Thus, the nearly constant terminal velocity of snow is also a consequence of the snowflake density being inversely proportional to diameter. The increase in terminal velocity from  $1.0 \text{ m s}^{-1}$  for dry snow to  $2.0 \text{ m s}^{-1}$  for wet or rimed snow is a result of the factor  $\rho_s D$  increasing by a factor of 4 for wet or rimed snow, leading to a factor of 2 increase in terminal velocity as a result of taking the square root.

### 3. Observations of visibility and snowfall rate from the NCAR Marshall field site

The NCAR winter test site was established with Federal Aviation Administration (FAA) funding in 1993 in support of NCAR's ongoing work in ground deicing. The initial studies focused on an evaluation of the performance of various types of snow gauges with various types of wind shielding in providing real-time, accurate liquid equivalent snowfall rates. During the winter of 1994/95, these studies expanded to include the use of visibility to measure snowfall intensity. In support of this work, two visibility sensors were installed at the Marshall site in the fall of 1994: a Vaisala FD12P and an HSS VPF-730. In March 1996, a Belfort Model 6220 Visibility Sensor also was installed. In addition to these

automatic sensors, manual estimates of visibility were made every 15 minutes during daylight hours by sighting on a row of evenly spaced telephone poles.

Liquid equivalent snowfall rate was measured in 1994/95 using ETI Instrument Systems 12" Automated Total Precipitation Rain and Snow Gauges, and Belfort Transmitting Precipitation Gauge Model 3000 snow gauges, one set with Alter shields and another set within a Wyoming shield. During the winter of 1995/96 a Geonor Model T-200 snow gauge with an Alter shield also was installed at the site. Manual measurements of liquid equivalent snow accumulation were made every 15 minutes by exposing a  $30 \text{ cm} \times 50 \text{ cm}$  pan to snowfall and weighing the pan before and after. Observations of crystal type, degree of riming, degree of snowflake aggregation, and mean and maximum sizes of the crystals and snowflakes were also made by an observer every 15 minutes using a magnifying glass and a ruler. Table 3 gives a list of the instrumentation deployed and the date of deployment. Table 4 gives a list of snow events for the winter of 1994/95, and Table 5 gives the corresponding table for the winter of 1995/96. The snow gauge and visibility data were acquired with a Campbell Scientific, Inc., CR10 datalogger and were recorded on various PCs located at the site. In this analysis 42 snow events were considered. These cases were not affected by fog or blowing snow. Wind starts to produce blowing snow at wind speeds greater than  $10 \text{ m s}^{-1}$  (Tabler 1984; Schmidt 1981). In most of the above cases, winds were less than  $10 \text{ m s}^{-1}$ .

To determine the best snow gauge and visibility sensor for our study, scatterplots of the manual measure-

TABLE 3. Instrumentation at NCAR Marshall test site (winter 1995/96).

Instrument/sensor/test equipment	Installation date	Operation date
12" ETI NOAH II Precipitation Gauge (Wyoming wind shield)	15 Aug 1995	6 Nov 1995
12" ETI NOAH II Precipitation Gauge (Lexan Alter wind shield)	15 Dec 1995	15 Dec 1995
12" ETI NOAH II Precipitation Gauge (Lexan Alter wind shield)	15 Dec 1995	15 Dec 1995
12" ETI NOAH II Precipitation Gauge (Lexan Alter wind shield)	6 Oct 1996	6 Nov 1995
12" ETI NOAH II Precipitation Gauge (Lexan Alter wind shield)	6 Oct 1996	7 Nov 1995
8" Belfort Model 3000 Precipitation Gauge (Wyoming wind shield)	15 Aug 1995	1 Oct 1995
8" Belfort Model 3000 Precipitation Gauge (Aluminum Alter wind shield and heat)	20 Sep 1995	10 Oct 1995
8" Belfort Model 3000 Precipitation Gauge (Aluminum Alter wind shield)	20 Sep 1995	1 Oct 1995
6.28" Geonor Model T-200 Precipitation Gauge (Steel Alter wind shield)	15 Aug 1995	1 Oct 1995
Campbell UDG01 Snow Depth Sensor	21 Oct 1995	21 Oct 1995
Campbell SR50 Snow Depth Sensor	7 Dec 1995	7 Dec 1995
Vaisala DRD 11A Precipitation Indicator	15 Aug 1995	1 Oct 1995
HSS VPF-730 Visibility/Pressure Weather Sensor	5 Oct 1995	21 Oct 1995
AES POSS (Precipitation Occurrence Sensor System)	10 Aug 1995	21 Oct 1995
Vaisala FD12P Visibility/Pressure Weather Sensor	10 Aug 1995	21 Oct 1995
STI LEDWI (Light Emitting Diode Weather Indicator)	10 Aug 1995	21 Oct 1995
Vaisala CT12K Ceilometer	17 Oct 1995	21 Oct 1995
Vaisala PTA-427A Pressure Sensor	1 Jun 1995	1 Oct 1995
Vaisala HMP35C Temperature/RH Probe	1 Jun 1995	1 Oct 1995
R.M. Young 05103 Wind Monitor at 3 m	21 Oct 1995	21 Oct 1995
R.M. Young 05103 Wind Monitor at 10 m	1 Jun 1995	1 Oct 1995
Belfort Model 6220 Xenon Strobe Visibility Sensor	12 Mar 1996	22 Mar 1996
Snow crystal video camera and rotating disk box	8 Dec 1995	8 Dec 1995

ments versus the automatic measurements were made. The 30- or 60-min liquid equivalent snowfall accumulation was calculated and compared to the 30- or 60-min accumulation determined from the manual pan method. Figure 2 presents the results from the best performing gauge-shield pair for the winter of 1994/95,

which is the ETI snow gauge in the Wyoming shield. The data show a good correspondence to the expected one-to-one line except on 19 April. This case was characterized by rain turning into snow. The data for 19 April show that the accumulation from the automatic measurement was much less than that of the manual

TABLE 4. The 1994/95 snow/precipitation events: Snow depth and liquid equivalent totals at Marshall test site, in inches.

Date	Liquid equivalent	Time (UTC)	Snowfall
3-4 Nov 1994	0.4	2300-0200	6
8-9 Nov 1994	0.4	1600-0100	6
14 Nov 1994	1.05	0400-1400	14
6 Dec 1994	0.07	1400-1900	1.5
8 Dec 1994	0.05	1200-1900	1
30-31 Dec 1994	0.22	1500-1900	5
3 Jan 1995	0.07	1400-1900	1.5
28-29 Jan 1995	0.45	2200-1300	6.5
10-12 Feb 1995	0.97	1900-1300	11
28 Feb-2 Mar 1995	0.22	0000-2300	3.5
6 Mar 1995	0.51	0400-2000	5
26-27 Mar 1995	0.07	0000-0000	1.5
28-30 Mar 1995	0.35	0000-0000	3.5
3 Apr 1995	Rain/freezing rain, 0.05	0000-0300	
10-11 Apr 1995	0.6	0600-0600	9
17 Apr 1995	0.5	Rain 0200-1300/ snow 0330-0509	
18 Apr 1995	0.2	0000-0600	1.5
19 Apr 1995	0.7	Rain 0000-0107/ snow 0107-1600	4
21-22 Apr 1995	0.42	Rain/snow 1310-1737 and 0416-0803	3
24 Apr 1995	0.19	0000-0400	1.0
26 Apr 1995	0.75	Rain 0200-0454/ snow 0454-1400	3.0
29-30 Apr 1995	Rain 0.36	0000-0000	
30 Apr 1995	Rain 0.32	0500-2300	

TABLE 5. The 1995/96 Marshall snowfall event summary.

Date	Liquid equivalent (in.)	Snowfall (in.)	Temperature	Max wind*	Comments/crystals
1–2 Nov 1995	0.13	3.0	15°–32°F	3605G10	Freezing drizzle, cold, dry snow
10 Nov 1995	0.18	1.5	23°–28°F	3506G22	Brief snow
27–28 Nov 1995	0.70	7.75	25°–32°F	1002G06	Heavy, wet snow
17 Dec 1995	0.05	1.0	26°–28°F	0203G8	Light snow
22 Dec 1995	0.05	1.4	19°–24°F	0404G10	Light snow
1 Jan 1996	0.20	2.8	21°–32°F	2304G8	Snow, gusting winds at beginning of event
4–5 Jan 1996	0.29	4.0	12°–32°F	0605G10	Moderate snow; dry, cold, graupel; then heavy rimed dendrites
17–18 Jan 1996	0.29	3.3	8°–39°F	0510G15	Arctic frontal passage; cold, dry snow; needles; dendrites, rimed
22–23 Jan 1996	0.07	1.8	12°–30°F	0903G08	Arctic front; cold, dry snow; heavy rimed dendrites
25–26 Jan 1996	0.47	6.5	6°–26°F	0405G15	Arctic front, upslope, irregular, moderate rime
30–31 Jan 1996	0.25	3.0	–10°–20°F	0402G8	Arctic air; cold, dry, light snow
26–28 Feb 1996	0.20	1.5	4°–24°F	0904G12	Light snow; rimed dendrites; arctic air
6 Mar 1996	0.30	1.5	5°–32°F	0906G12	Light snow; dendrites; heavy rime
14 Mar 1996	0.90	7.0	31°–32°F	3405G10	Rain turning to wet snow, needles, dendrites, heavy rime, steady
17 Mar 1996	0.08	1.0	30°–32°F	3610G20	Short period of moderate-to-heavy snow; heavy rimed aggregates
24 Mar 1996	0.60	8.0	13°–32°F	0905G15	Rain turning to snow; dendrites, heavy rime, cold, moderate-to-heavy snow
4–5 Apr 1996	0.72	5.0	23°–39°F	3605G25	Rain 0200–0800, snow 0800–1200 and 2200–1500 UTC
13 Apr 1996	0.14	2.0	32°–33°F	3610G20	Short periods of light snow, moderate rimed dendrites, plates, 15-min aggregates
22 Apr 1996	0.34	1.0	30°–36°F	3602G4	Light rain/light snow

\* Direction (compass degrees/10), maximum sustained wind speed ( $\text{mi h}^{-1}$ ), and maximum gust ( $\text{mi h}^{-1}$ ), coded as DDWWGWW.

measurement. Analysis of the automatic gauge data showed that the total storm accumulation was close to that measured manually, but that a large snow “dump” occurred during midmorning. This dump occurred because snow accumulating on the sidewalls of the gauge later fell into the gauge as a result of solar heating that melted the ice bond between the snow and the sidewalls of the gauge. The snow accumulating on the sidewalls

is not weighed by the gauge, and thus the real-time rate is reduced considerably. Thus, the automatic snow gauge measurements from 19 April are suspect and have been deleted. The remaining data from the ETI gauge are used in this analysis to calculate snowfall rates for the winter of 1994/95.

The comparison of HSS visibility and manual visibility measurements for the winter of 1994/95 (Fig. 3) shows good agreement, validating both methods. The Vaisala visibility measurements, however, did not show as good a correlation with the manual visibility measurements (not shown).

Similar scatterplots for liquid equivalent snowfall and visibility during the winter of 1995/96 show the best automatic gauge for this winter to be the Geonor gauge (Fig. 4), and the best visibility instrument again to be the HSS (Fig. 5). During the winter of 1995/96, an event similar to that of 19 April 1995 occurred on 14 March 1996 in which rain turned to snow and significant sidewall accumulation occurred. It was decided to substitute the manual snowfall measurements for automatic snow gauge measurements for this day only.

Plots of visibility versus liquid equivalent snowfall rate for the winter of 1994/95 and the winter of 1995/96 are shown in Figs. 6 and 7, respectively. The HSS visibility data are collected every minute and averaged over the time period between tips of the ETI or Geonor gauges. The ETI gauge increments its accumulation every 0.025 cm of liquid equivalent snow accumulation,

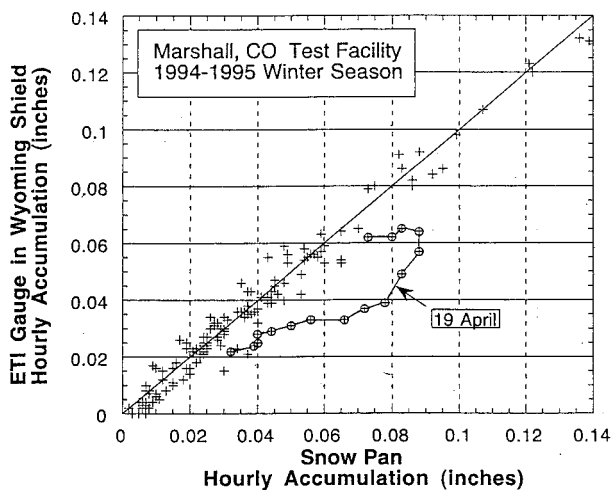


FIG. 2. Scatterplot of hourly precipitation amounts from the ETI gauge in the Wyoming shield and the manual snow pan measurements for the 177 h for which observations were made concurrently during the winter of 1994/95.

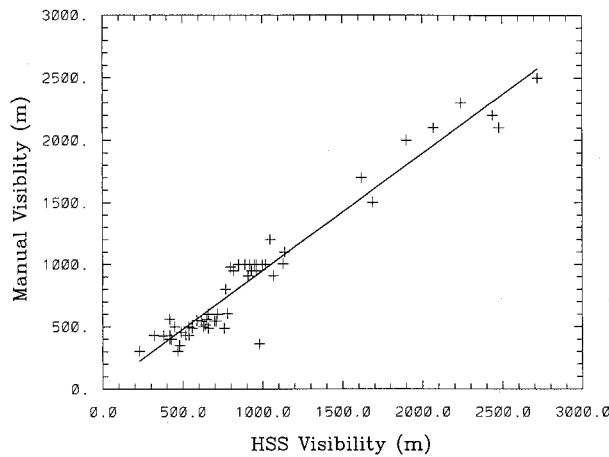


FIG. 3. Manual visibility (m) vs 1-min average HSS VPF-730 visibility (m) measured at the same time as the manual observation. Data collected during the winter of 1994/95 at the NCAR Marshall field site. The correlation coefficient was 0.9677 and the linear regression line is  $y = 0.943x + 7.702$ .

while the Geonor increments every 0.0025 cm. In the case of the Geonor an accumulation increment of 0.0125 cm was used in order to have a reasonable time interval for averaging. Typical times between tips ranged from 1 min, yielding a snowflake rate of  $8 \text{ mm h}^{-1}$ , to 60 min, for a rate of  $0.13 \text{ mm h}^{-1}$ . The averaging error introduced by the 1-min resolution of the visibility data is most pronounced at high snowfall rates because of the short time between accumulation tips. This error is estimated to be less than 10%.

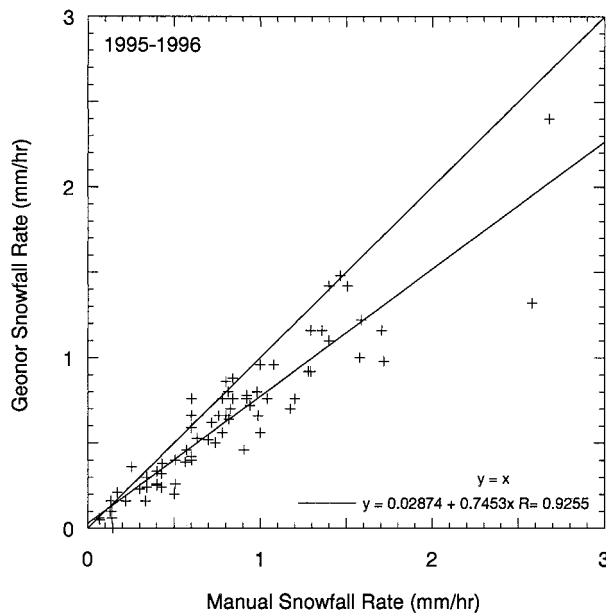


FIG. 4. Scatterplot of the Geonor snowfall rate in  $\text{mm h}^{-1}$  and manual snow pan rates for either 15 or 30 min during the winter of 1995/96. Data from 14 Mar 1996 omitted due to sidewall collection problem. The correlation coefficient equals 0.93.

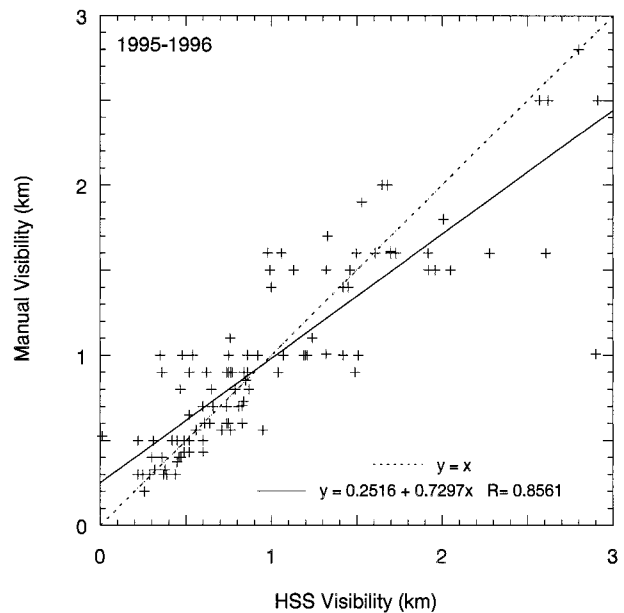


FIG. 5. Same as Fig. 3 but for the winter of 1995/96. The correlation coefficient equals 0.86.

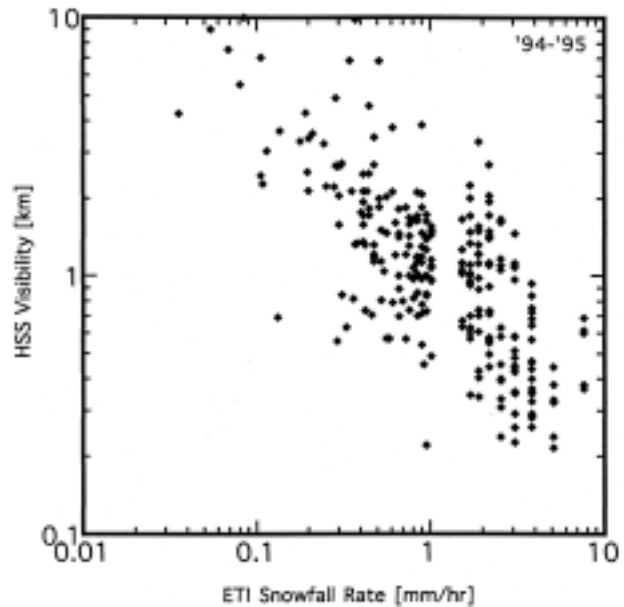


FIG. 6. HSS VPF-730 visibility (km) vs ETI liquid equivalent snowfall rate ( $\text{mm h}^{-1}$ ) in the Wyoming shield at the NCAR Marshall test site from the winter of 1994/95. The snowfall rates were calculated for every tip (0.025 cm) of the snow gauge, and the corresponding HSS data averaged between tips. The data in the plot cover all periods of snow between 1 Feb and 25 Apr 1995, excluding 19 Apr because of problems of sidewall collection of snow in the ETI gauge; and 6 Mar 1995 from 1720–2324 UTC and 10 April 1710–2010 UTC because of problems during bright conditions (intense scattering of sunlight from new-fallen snow) with the HSS visibility sensor.

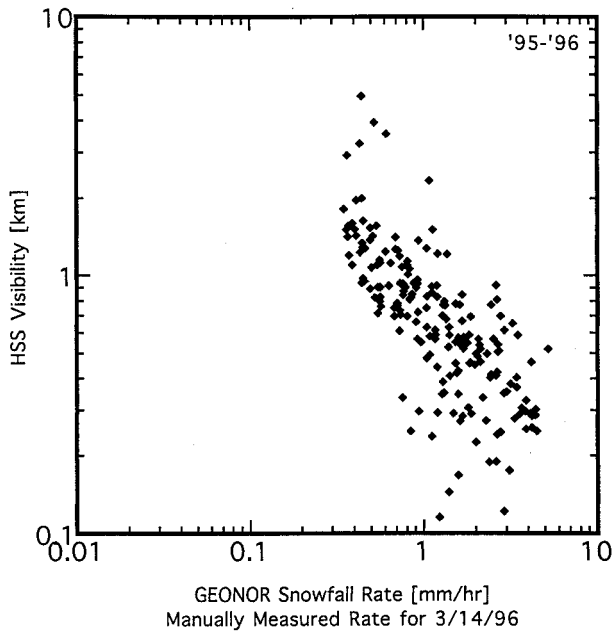


FIG. 7. Same as Fig. 6 but for the winter of 1995/96 and for the Geonor snow gauge. Snowfall rates were calculated at every 0.0125 cm of accumulation in the gauge. Manual snowfall rates were substituted for 14 Mar 1996 because of snow collecting on the sidewalls of the Geonor gauge.

A large amount of scatter is evident in the relationship between snowfall rate and visibility (Figs. 6, 7), especially considering the log–log scale employed. For example, the visibility at a constant liquid equivalent snowfall rate of  $2.0 \text{ mm h}^{-1}$  ranges from 0.3 to 3.0 km, or from heavy to light snowfall intensity, similar to the observations from the accidents. Similarly, the liquid equivalent snowfall rate for a constant visibility of 1.0 km ranges from 0.8 to  $3 \text{ mm h}^{-1}$ . Thus, the Marshall observations confirm the large scatter in visibility for a given liquid equivalent snowfall rate as was observed near the time of the accidents. In order to understand this result further, theoretical relationships between liquid equivalent snowfall rate and visibility are developed in the next section and are compared to the observations in section 5.

#### 4. Theoretical considerations

In order to understand the cause of the scatter in the liquid equivalent snowfall rate versus visibility plots, theoretical expressions for the relationship between liquid equivalent snowfall rate and visibility for dry and wet or rimed snow and for 27 different ice crystal types are derived below. Dry and wet and/or rimed snowflakes are considered in section 4a and the 27 different crystal types in section 4b.

##### a. Theoretical relationship between visibility and liquid equivalent snowfall rate for snowflakes

Optical methods for measuring visibility are sensitive to the cross-sectional area of the particles in the beam. In the following, a theoretical expression that relates visibility to the snowflake size distribution and particle density is developed. Let us assume a snow size distribution specified using a gamma size distribution (Braham 1990):

$$N(D) = N_0 D^m \exp(-\Lambda D), \quad (2)$$

where  $\Lambda$  is the slope of the size distribution,  $N_0$  is the y intercept,  $D$  is the snowflake particle diameter, and  $m$  is the order of the gamma size distribution. The value of  $m$  determines the shape of the distribution. Most snow spectra have been observed to be exponential (Braham 1990), for which  $m = 0$ . Individual snowflakes are assumed to be spherical in this equation. Depending on the amount of riming, aggregation, and/or melting, the bulk density of a snowflake varies between  $0.005$  and  $0.2 \text{ g cm}^{-3}$  (Fig. 1).

Meteorological visibility (Vis) during the day can be related approximately to extinction coefficient using the Koschmieder relation (Middleton 1954; see section 6a for a derivation):

$$\text{Vis} = 3.912/\sigma \text{ cm}, \quad (3)$$

where  $\sigma$  is the path-averaged extinction coefficient of an ensemble of snow particles per unit volume ( $\text{cm}^2 \text{ cm}^{-3}$ ). The extinction coefficient accounts for scattering and absorption by particles in the volume and is defined as

$$\sigma = \frac{2\pi}{4} N_0 \int_0^\infty D^2 D^m \exp(-\Lambda D) dD \quad (4)$$

$$= \frac{\pi N_0 \Gamma(m+3)}{2\Lambda^{m+3}} \text{ cm}^2 \text{ cm}^{-3} \quad (5)$$

for the size distribution given in Eq. (2). For visible wavelengths, absorption generally is small. Here  $\Gamma()$  is the complete gamma function (Press et al. 1986). The factor of 2 in Eq. (4) is due to diffraction of light around an object, resulting in a scattering cross-sectional area that is twice the physical cross-sectional area. When Eqs. (3) and (5) are combined, Vis can be expressed as

$$\text{Vis} = 2.49 \frac{\Gamma(m+1)(3.67+m)^2}{\Gamma(m+3)D_0^3 N_t} \text{ cm} \quad (6)$$

$$= 2.49 \frac{\Gamma(m+1)\Lambda^2}{\Gamma(m+3)N_t} \text{ cm}, \quad (7)$$

where  $N_t$  is the number concentration of snow particles per unit volume and  $D_0$  is the median particle diameter, that is, half the mass of the particle size distribution is in particles less than  $D_0$ . In general,  $N_t$  and  $D_0$  increase with snowfall rate and, hence, snowfall rate is inversely proportional to visibility for a given  $m$ . Note that wind speed is not considered in this equation; thus the speed

at which the particles are moving either vertically or horizontally at a given instant has no impact on the measured visibility. The net vertical velocity of a snow particle, however, will have an impact on the calculated snowfall rate from a given distribution.

If the snow particle size distribution is assumed to be exponential ( $m = 0$ ), then Eqs. (6) and (7) reduce to

$$\text{Vis} = \frac{16.77}{D_0^2 N_t} \text{ cm} \tag{8}$$

$$= \frac{1.245 \Lambda^2}{N_t} \text{ cm.} \tag{9}$$

For the same snow size distribution that was presented in Eq. (2), the snowfall rate can be written as

$$S = \frac{\pi \rho_s N_0 \Gamma(m + 4) \bar{V}_t}{6.0 \Lambda^{m+4}} \text{ cm s}^{-1}, \tag{10}$$

where  $\bar{V}_t$  is the average fall velocity for the snow particle size distribution ( $\text{cm s}^{-1}$ ) and  $\rho_s$  is the mean snow particle density ( $\text{g cm}^{-3}$ ). Since the density of water is  $1 \text{ g cm}^{-3}$ , the units of Eq. (10) also can be written as grams per centimeter squared per second.

The variation in snowfall rate and visibility for a wide range of possible values of  $N_t$ ,  $D_0$ , and  $\rho_s$  can be examined using Eq. (10) and the visibility Eq. (7). Figure 8a shows model computations of visibility as a function of snowfall rate for an exponential size distribution ( $m = 0$ ) in which the parameters  $N_t$ ,  $D_0$ , and  $\rho_s$  are varied between realistic values. Specifically,  $N_t$  is varied between  $0.1$  and  $10 \text{ L}^{-1}$ ,  $D_0$  between  $0.1$  and  $1 \text{ cm}$  (Braham 1990), and  $\rho_s$  between  $0.01$  and  $0.2 \text{ g cm}^{-3}$ , while a mean snow terminal velocity of  $1 \text{ m s}^{-1}$  is assumed. The results show that a large range of visibility values are possible for a given snowfall rate. For example, the visibility ranges from  $0.3$  to nearly  $10 \text{ km}$  at a snowfall rate of  $0.5 \text{ mm h}^{-1}$ , and from  $0.1$  to  $2 \text{ km}$  for a snowfall rate of  $2 \text{ mm h}^{-1}$ . Similarly, for a given visibility, snowfall rate can vary by nearly two orders of magnitude. For instance, a visibility of  $1 \text{ km}$  can occur for snowfall rates from  $0.05$  to over  $8 \text{ mm h}^{-1}$ . This wide scatter suggests that it is not possible to estimate snowfall rate from visibility alone without some simplifying assumptions or knowledge about  $N_t$  and  $D_0$ ,  $\rho_s$ , or crystal type. If, for instance,  $\rho_s$  is fixed at  $0.05 \text{ g cm}^{-3}$ , the plot in Fig. 8b is obtained. The scatter clearly has been reduced, with a much more defined curve. In this case, the visibility varies only between  $0.2$  and  $1.0 \text{ km}$  at  $2.5 \text{ mm h}^{-1}$  liquid equivalent snowfall rate.

To illustrate the effect of bulk density on visibility for a given snowfall rate, the snowfall rate is fixed at  $2 \text{ mm h}^{-1}$  and the bulk density is varied between  $0.01$  and  $0.2 \text{ g cm}^{-3}$  in Fig. 9. The parameters  $N_t$  and  $D_0$  are allowed to vary randomly as given above, consistent with a  $2 \text{ mm h}^{-1}$  rate. The visibility is shown to be nearly directly proportional to bulk density at the constant snowfall rate, with the visibility increasing from

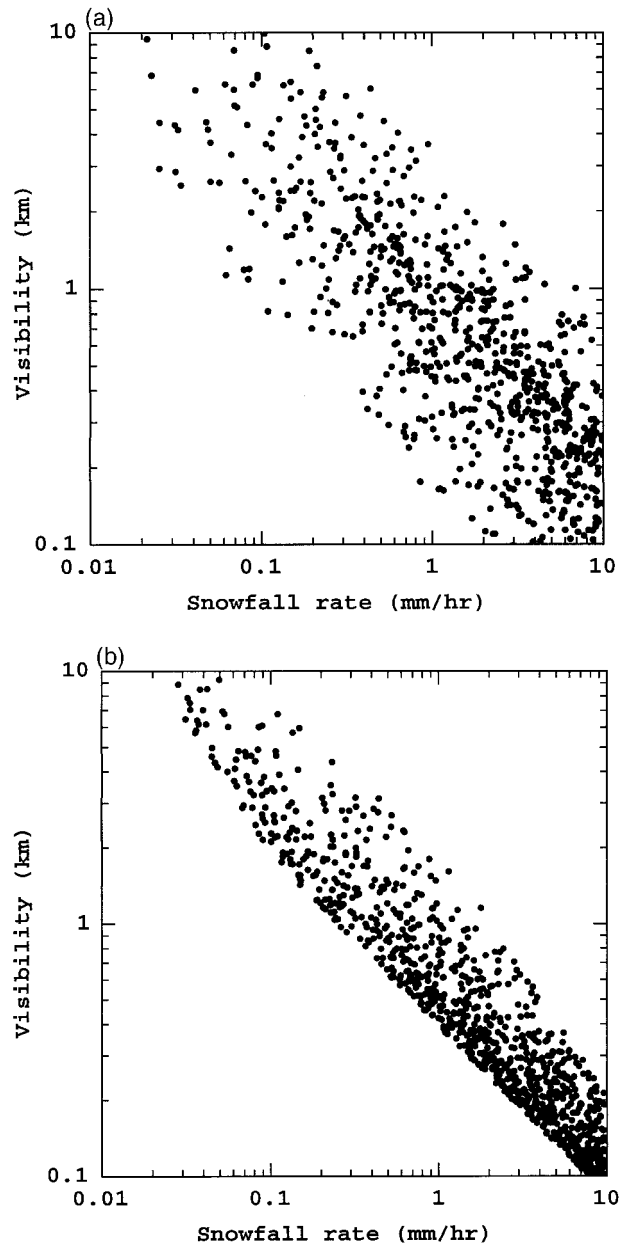


FIG. 8. (a) Visibility as a function of liquid equivalent snowfall rate calculated using Eqs. (8) and (10) by allowing  $N_t$  to vary between  $0.1$  and  $10 \text{ L}^{-1}$ ,  $D_0$  between  $0.1$  and  $1 \text{ cm}$ , and  $\rho_s$  between  $0.01$  and  $0.2 \text{ g cm}^{-3}$  assuming a snowflake fall velocity of  $1 \text{ m s}^{-1}$ . (b) Same as (a) but the mean bulk density of snow particles is fixed at  $\rho_s = 0.05$  while  $N_t$  and  $D_0$  varied as in (a).

$0.10 \text{ km}$  at a bulk density of  $0.01 \text{ g cm}^{-3}$  to nearly  $2 \text{ km}$  for a bulk density of  $0.2 \text{ g cm}^{-3}$ . The former density represents low-density snowflake aggregates, while the latter is representative of rimed or wet snowflakes.

Consider now the inverse relationship between diameter and snowflake density discussed in the previous section:

$$\rho_s D = C_3 \text{ g cm}^{-2}, \tag{11}$$

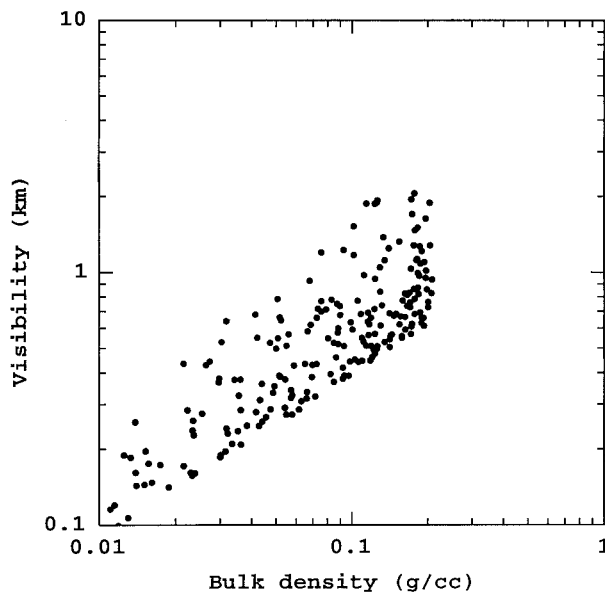


FIG. 9. Theoretical visibility as a function of bulk snow density for a fixed snowfall rate of  $2 \text{ mm h}^{-1}$ , allowing  $N_t$  and  $D_0$  to vary consistent with a  $2 \text{ mm h}^{-1}$  snowfall rate.

where  $C_3$  is a constant whose value depends on whether the snow is dry or wet/rimed. Using this relationship the following equation for snowfall rate can be formed:

$$S = C_3 \frac{\pi}{6} N_t \frac{\Gamma(m+3) \bar{V}_t}{\Gamma(m+1) \Lambda^2} \text{ cm s}^{-1}. \quad (12)$$

By combining the equation for visibility [Eq. (7)] and the snowfall rate Eq. (12), the following relationship is found:

$$S = \frac{1.3C_3 \bar{V}_t}{\text{Vis}} \text{ cm s}^{-1}, \quad (13)$$

where  $V_t$  is in centimeters per second, Vis is in centimeters,  $C_3$  is in grams per centimeter squared, and  $S$  is in centimeters per second. This simple relationship shows that snowfall rate is inversely proportional to visibility if the snowflake density is inversely proportional to snowflake diameter. Note also that the snowfall rate is independent of the snowflake size distribution. This independence occurs because the integrals over size distribution for visibility and snowfall rate cancel each other out [both are equal to  $\int_0^\infty D^2 D^m \exp(-\Lambda D) dD$ ]. As discussed above, this functional relationship is true for snowflake aggregates, with the value of  $C_3$  dependent on whether the snowflakes are dry, wet, or rimed.

In Fig. 10 a plot of Eq. (13) is presented for values of  $C_3$  and terminal velocity that are representative of dry snow ( $0.017 \text{ g cm}^{-2}$  and  $100 \text{ cm s}^{-1}$ , respectively), and for values of  $C_3$  and terminal velocity that are representative of wet or rimed snow ( $0.072 \text{ g cm}^{-2}$  and  $200 \text{ cm s}^{-1}$ , respectively) (Rogers 1974). The curves for

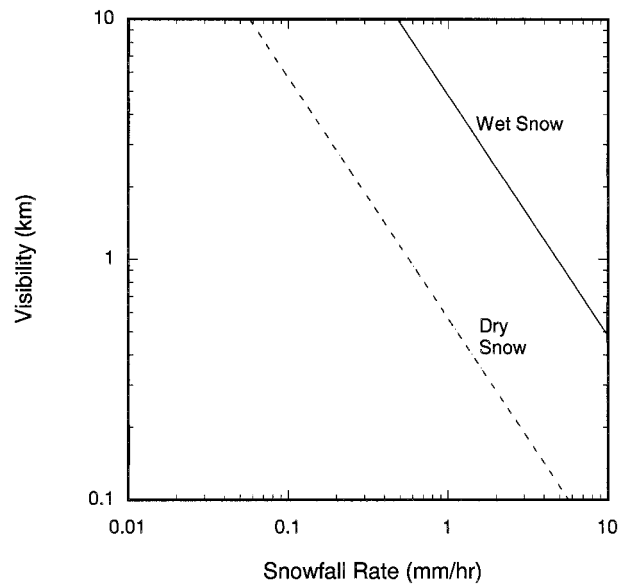


FIG. 10. Theoretical relationship between visibility and snowfall rate for dry and wet aggregated snow. The values of  $C_3$  and terminal velocity used for the dry snow curve are  $0.017 \text{ g cm}^{-2}$  and  $100 \text{ cm s}^{-1}$ , respectively, and the values for the wet snow curve are  $0.072 \text{ g cm}^{-2}$  and  $200 \text{ cm s}^{-1}$ , respectively.

“dry”<sup>3</sup> and “wet”<sup>4</sup> snowflakes show the expected inverse relationship between visibility and snowfall rate from Eq. (13). The increase in terminal velocity for wet snow is based on the fact that wet and/or rimed snowflake aggregates typically fall twice as fast as dry snowflake aggregates do (Magono and Nakamura 1965; Zikmunda and Vali 1972). The visibility for a snowfall rate of  $2.0 \text{ mm h}^{-1}$  ranges from  $0.3 \text{ km}$  for dry snow to  $2.6 \text{ km}$  for wet or rimed snow. Thus, the variations in these curves at  $2 \text{ mm h}^{-1}$  span the visibility-defined snowfall intensities of light, moderate, and heavy, despite the constant liquid equivalent snowfall rate.

This wide range in visibility for a given snowfall rate is produced by two factors: 1) the smaller cross-sectional area of wet and/or rimed snowflake aggregates compared with that of unrimed and/or dry snowflake aggregates of the same mass and 2) the higher terminal velocity of wet and/or rimed snowflake aggregates compared with that of the unrimed and/or dry snowflake aggregates of the same mass. Both of these factors contribute to producing a wide range of visibilities for the same absolute snowfall rate. As will be shown in the next section, this result is consistent with the data analysis conducted at Marshall presented in the previous section and with the analysis of snowfall conditions during previous ground deicing accidents (Rasmussen et al. 1995). Most of the accidents occurred at temperatures

<sup>3</sup> Dry snow is assumed to be unmelted and unrimed.

<sup>4</sup> Wet snow includes partially melted snow and/or rimed snow.

close to 0°C, consistent with wet and/or rimed snowflakes.

*b. General theoretical relationship between visibility and snowfall rate for various snow crystal types*

As mentioned in section 2, individual snow crystals typically have bulk densities that are nearly constant with size (see Table 2). Thus, the simple form of Eq. (13) is not possible for single crystals. However, various literature-reported power-law relationships between crystal diameter and cross-sectional area, volume, and terminal velocity (Table 2) may be used to derive a general relationship between visibility and snowfall rate for a variety of snow crystal types. The following power-law relationships are assumed:

- 1)  $A_c = aD^b$ ,
- 2)  $V = cD^d$ ,
- 3)  $\rho_s = eD^f$ , and
- 4)  $V_t = gD^h$ ,

where  $A_c$  is the cross-sectional area of a crystal perpendicular to the line of sight,  $V$  is the volume of the crystal,  $a$ – $h$  are coefficients and exponents, and  $D$  is the crystal diameter. Following the derivation of the relationship between visibility and the type and number of particles presented in the previous section, the optical cross section or extinction coefficient for an ensemble of snow crystals of cross-sectional area  $A_c$  can be written as

$$\sigma = 2N_0 \int_0^\infty A_c D^m \exp(-\Lambda D) dD. \quad (14)$$

Using the above power law for the cross-sectional area, the extinction coefficient can be solved for

$$\sigma = \frac{2aN_0\Gamma(m+b+1)}{\Lambda^{m+b+1}} \text{cm}^2 \text{cm}^{-3}, \quad (15)$$

and the visibility is

$$\text{Vis} = \frac{3.91\Lambda^{m+b+1}}{2aN_0\Gamma(m+b+1)} \text{cm}. \quad (16)$$

In the same manner, the snowfall rate equation can be written using the above power-law relationships as

$$S = \frac{N_0ecg\Gamma(f+d+h+m+1)}{\Lambda^{f+d+h+m+1}} \text{cm s}^{-1}. \quad (17)$$

The values of  $a$ ,  $b$ ,  $c$ ,  $d$ ,  $e$ ,  $f$ ,  $g$ , and  $h$  for 27 crystal types and dry and wet snow can be found in Table 2 using cgs units. The values in the table are relevant to conditions at 1000 mb and were obtained primarily from the work of Heymsfield and Kajikawa (1987), with additional input on selected crystal types from Heymsfield (1972), Mitchell et al. (1990), Jayaweera and Cottis (1969), Jayaweera and Ohtake (1974), Iwai (1973), Zikmunda and Vali (1972), and Davis (1974).

Substituting the above visibility equation into the snowfall equation results in a general equation that relates snowfall rate to visibility for various crystal types:

$$S = \frac{3.91ecg\Gamma(f+d+h+m+1)\Lambda^{b-f-d-h}}{2a\text{Vis}\Gamma(b+m+1)} \text{cm s}^{-1}, \quad (18)$$

where Vis is in centimeters. Assuming an exponential size distribution ( $m = 0$ ), the above equation can be written as

$$S = \frac{3.91ecg\Gamma(f+d+h+1)\Lambda^{b-f-d-h}}{2a\text{Vis}\Gamma(b+1)} \text{cm s}^{-1}. \quad (19)$$

The above theoretical expression assumes that the crystals fall with their longest dimension oriented horizontally. Experimental tank studies by Willmarth et al. (1964) and Jayaweera and Mason (1965) show that disks and columns start shedding rear eddies at Reynolds numbers of 100 and 50, respectively. The onset of shedding causes the crystal to flutter about the horizontal and eventually leads to unstable motions. For typical atmospheric conditions of 700 mb and  $-10^\circ\text{C}$ , the above Reynolds number translates into platelike crystal sizes of 5 mm and columnar crystal diameters of 1.4 mm. Typical crystal sizes for both platelike and columnar crystals are both less than 5- and 1.4-mm diameter, respectively, so that unstable hydrodynamic motions are not expected to have a significant effect on the theoretical estimates of visibility using Eq. (19) above. Observations by Zikmunda and Vali (1972) show that columnar crystals only deviate from a horizontal orientation by  $15^\circ$  or less for crystal sizes up to 0.5-mm diameter, consistent with the above results. On the other hand, Zikmunda and Vali (1972) frequently observed rotation of columnar crystals in a horizontal plane. Thus, the assumption that columnar crystals are oriented perpendicular to the viewer at all times is not correct. Therefore the effective cross-sectional area of the columnar crystals in Eq. (14) needs to be reduced by a factor of  $2/\pi$ , which is derived by integrating the cross-sectional area through a half revolution. In the figures that follow, this reduction in cross-sectional area has been taken into account.

Equation (19) can be reduced to Eq. (13) for dry spherical snowflakes if one sets  $a = \pi/4$ ,  $b = 2$ ,  $c = \pi/6$ ,  $d = 3$ ,  $e = 0.017 \text{ g cm}^{-2}$ ,  $f = -1$ ,  $g = 100 \text{ cm s}^{-1}$ , and  $h = 0$ . Both Eqs. (19) and (13) show that visibility for a given snowfall rate is increased as the snowflake density increases, the cross-sectional area is reduced, and the terminal velocity increased. Thus, compact crystals of high density and high fall velocity will result in the highest visibility for a given snowfall rate.

To apply Eq. (19), the slope of the snow crystal size distribution  $\Lambda$  needs to be specified. Aircraft measurements of ice crystal size distributions have found that  $\Lambda$  typically varies between 10 and  $30 \text{ cm}^{-1}$  (Braham 1990; Houze et al. 1979) for a wide variety of crystal

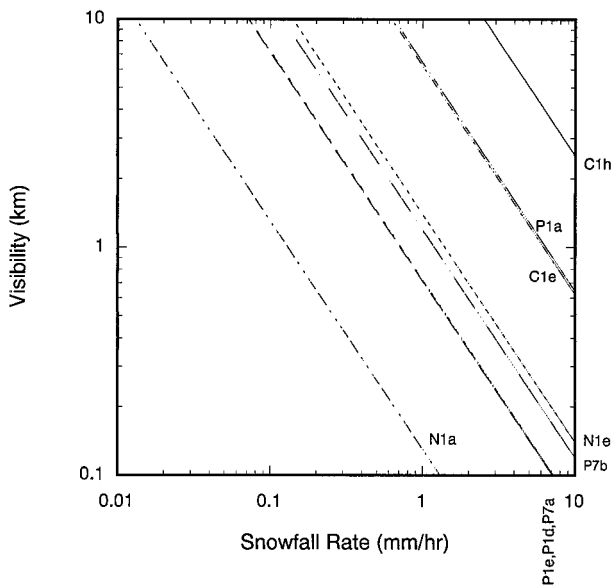


FIG. 11. Predicted visibility-snowfall relationship for unrimed crystal types using Eq. (19) with appropriate values of the various constants from Table 2. Crystal types represented are dendrites (P1e), stellars (P1d), hexagonal plates (P1a), thick plates (C1h), short columns (C1e), elementary needles (N1a), long columns (N1e), radiating assemblages of dendrites (P7b), and radiating assemblages of plates (P7a).

types and storms. In the following analysis a mean value of  $\Lambda = 20 \text{ cm}^{-1}$  is used.

Figure 11 presents the predicted visibility-snowfall rate relationship for the following seven unrimed crystal types on a log-log plot: dendrites (P1e), stellars (P1d), hexagonal plates (P1a), thick plates (C1h), short columns (C1e), elementary needles (N1a), long columns (N1e), radiating assemblages of dendrites (P7b), and radiating assemblages of plates (P7a). Note that the curves follow the same slope due to the inverse relationship between snowfall rate and visibility in Eq. (19). Also note the wide variation in visibility for a given snowfall rate for the different crystal types. The highest visibility for a given precipitation rate occurs for the thick plates (C1h), the hexagonal plates (P1a), and the short columns (C1e). These crystal types are very compact in shape, have a density near pure ice, and have a relatively high terminal velocity, leading to a relatively high visibility for a given precipitation rate.

Dendrites (P1e), stellars (P1d), and radiating assemblages of dendrites (P7b) are associated with moderate visibilities for a given precipitation rate, reflecting their less compact shape, lower density, and lower terminal velocity compared with those of the compact crystals mentioned above.

The lowest visibility for a given precipitation rate occurred for the elementary needles (N1a), reflecting the relatively large surface area-to-mass ratio for these crystal types, the lower density, and the relatively low terminal velocities.

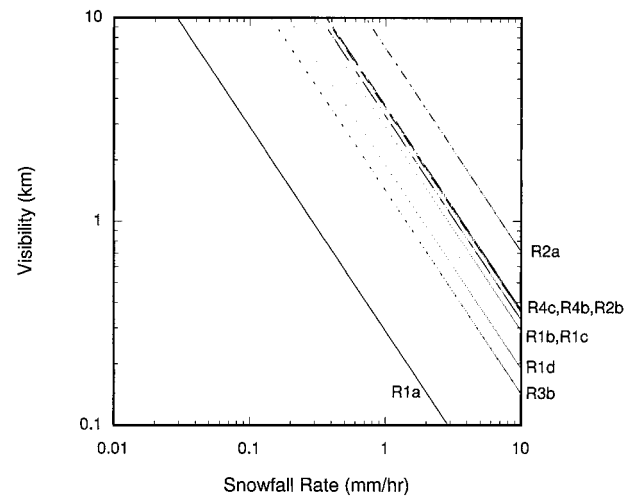


FIG. 12. Same as Fig. 11 but for rimed crystal types. Crystal types represented are conical graupel (R4c), lump graupel (R4b), densely rimed stellar (R2b), densely rimed plate (R2a), rimed plate (R1c), rimed long column (R1b), rimed stellar (R1d), heavily rimed dendrite (R3b), and rimed elementary needle (R1a).

The above curves suggest that visibility can vary by over two orders of magnitude from variations in crystal type alone. The theoretical curves for rimed crystals (Fig. 12) show that rimed dendrites, stellars, columns, and needles all are associated with a factor of 3–4 increased visibility for a given precipitation rate when compared with the unrimed crystal, primarily from an increase in terminal velocity as a result of riming (see Table 2).

Graupel (R4c, R4b) has nearly the highest associated visibility of any rimed particle because of the compact shape and high terminal velocity. Aggregated crystals (snowflakes) have a relatively low associated visibility for a given precipitation rate when compared with single crystals (see Fig. 10 in the previous section). However, wet or rimed snowflakes are associated with one of the highest visibilities of all crystal types because of the factor of 2 increase in terminal velocity and factor of 4 increase in the product  $\rho_s D$ , leading to a factor of 8 increase in visibility for a given precipitation rate when compared with dry snow [see Eq. (13) and Fig. 10]. Various other crystal types with various types of branching are shown in Fig. 13, with the curves falling midway between the dry and wet snowflake curves.

The above analysis shows that visibility for a given precipitation rate depends critically on the type of crystal, the degree of aggregation, and the degree of riming and melting, with riming, melting, and compact, dense crystals leading to the highest visibilities for a given precipitation rate.

Also note that nearly all of the single crystal curves have a higher visibility for a given snowfall rate than does dry snow. This finding partially reflects the typically loose packing that occurs in snowflake aggregates, resulting in larger cross-sectional areas for a snowflake

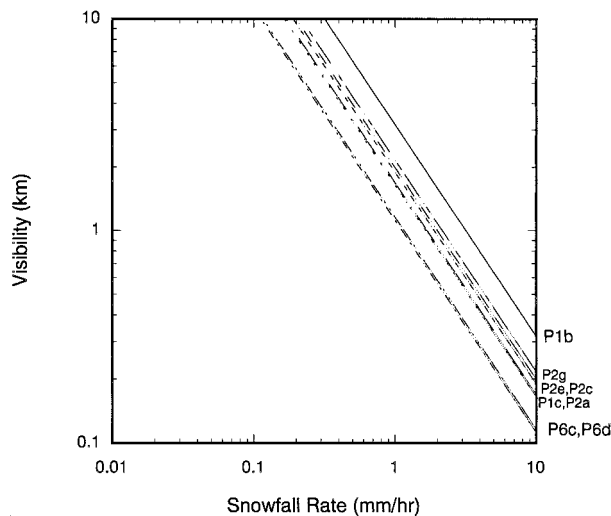


FIG. 13. Same as Fig. 11 but for the following crystal types: hexagonal plate with sectorlike branches (P1b), hexagonal plate with broad branches (P1c), stellar with end plates (P2a), dendrite with end plates (P2c), plate with extensions (P2e), plate with dendritic extensions (P2g), stellar with spatial plates (P6c), and stellar with spatial dendrites (P6d).

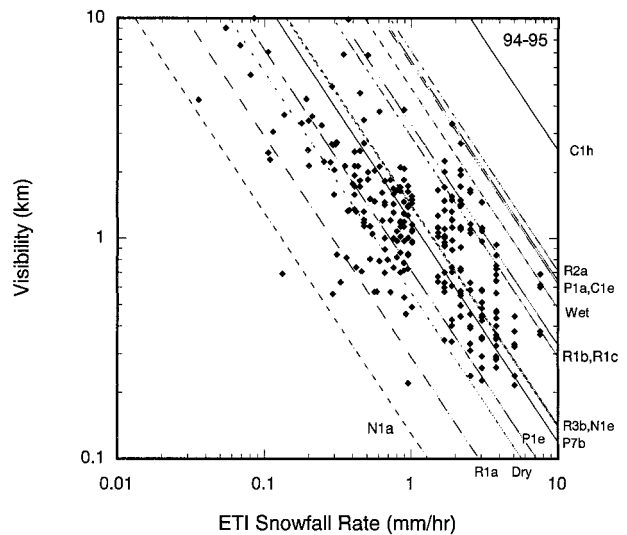


FIG. 14. Theoretical visibility–snowfall relationships from Eq. (19) for unrimed, rimed, and dry and wet spherical snowflakes compared to observed visibility–snowfall data from the NCAR Marshall field site collected during the winter of 1994/95. Visibility data were obtained from the HSS VPF-730 visibility instrument and snowfall rate is from an ETI snow gauge with a Wyoming shield. The snowfall rates were calculated for every tip (0.025 cm) of the snow gauge and the corresponding HSS visibility data averaged over the time between tips.

consisting of  $n$  crystals than for the  $n$  individual crystals by themselves.

**5. Comparison of observations with theory**

*a. Comparison of NCAR Marshall observations with theory*

A comparison of the above theory with data from the winter of 1994/95 (Fig. 14) and the winter of 1995/96 (Fig. 15) shows that most of the data points fall within the theoretical curves described in the previous section. To understand this result further, data from typical snow events during these two years are presented below and compared with the relevant theoretical curves. Since most storms have a mixture of crystal types, we present individual storms rather than data stratified by crystal type.

1) CASE 1: 6 MARCH 1995

Key feature—Variety of crystal types and riming leading to scatter in the visibility–snowflake rate relationship

Temperature range—0° to –8°C

Range of wind speeds—0 to 8 m s<sup>-1</sup>

Crystal types and size ranges—Heavily rimed dendrites and needles, light to moderately rimed sector plates, stellars, and radiating assemblages of dendrites

Degree of riming—Light to heavy

Degree of aggregation and maximum aggregate size—None

Range of snowflake terminal velocities—

1.2–1.5 m s<sup>-1</sup>

Range of snowfall rates—0.0 to 8.0 mm h<sup>-1</sup>

Temperatures started out near 0°C at 0500 UTC and fell gradually to –3°C by 1600 UTC. Wind speeds during this period ranged from 0 to 4 m s<sup>-1</sup>, and the crystal types between 1400 and 1600 UTC were needles and

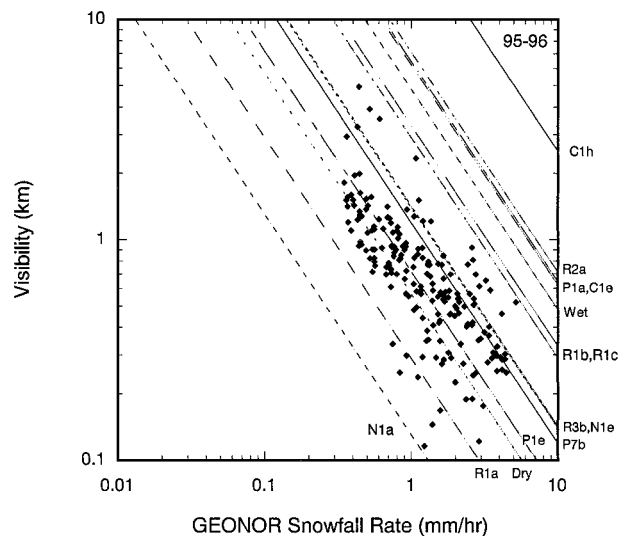


FIG. 15. Same as Fig. 14 but for the winter of 1995/96 using Geonor snow gauge data instead of ETI data. Geonor rates were calculated every 0.0125 cm of liquid equivalent snow accumulation.

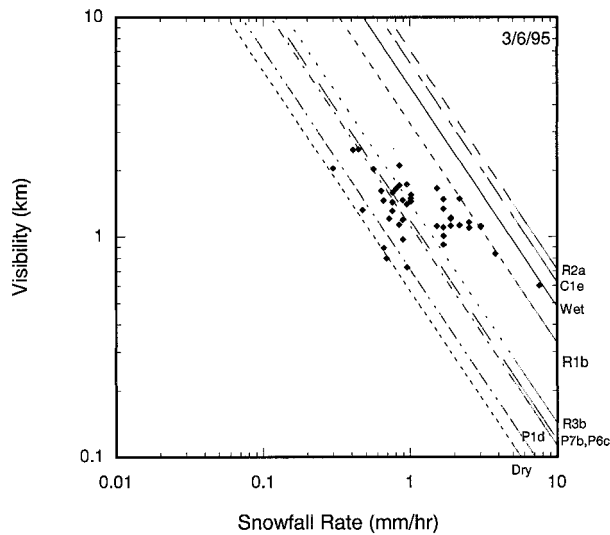


FIG. 16. Theoretical visibility–snowfall relationships from Eq. (19) compared to the observed visibility–snowfall data from 6 Mar 1995. The theoretical curves correspond to the crystal types observed for this event.

heavily rimed dendrites less than 2 mm in diameter, with little to no aggregation. Between 1600 and 1700 UTC the temperature dropped to  $-7.5^{\circ}\text{C}$  and the wind speed increased to nearly  $8\text{ m s}^{-1}$  in association with a frontal passage. During this same time period, the crystal type changed to light to moderately rimed sector plates, stellars, and radiating assemblages of dendrites. The snowfall rate versus visibility plot (Fig. 16) shows that the data fall within the relevant theoretical curves: stellars (P1d), densely rimed dendrites (R3b), radiating assemblages of plates (P7a), dendrites (P7b), and rimed long columns (R1b).

The extremely high snowfall rate of  $8\text{ mm h}^{-1}$  is associated with heavily rimed crystals and with a visibility of 0.6 km, which is only moderate snow intensity based on visibility. At a visibility of 1.25 km, precipitation rate varied between  $0.4\text{ mm h}^{-1}$  and  $3.0\text{ mm h}^{-1}$ , which is nearly an order of magnitude variation under light snowfall conditions as defined by a visibility of 1.25 km. At a precipitation rate of  $1.0\text{ mm h}^{-1}$ , the visibility varied between 0.7 and 2 km (moderate to light snowfall). Thus, the variation of crystal type and degree of riming in this case led to a large scatter in the snowfall rate–visibility relationship on this day. Of particular note was the presence of an extremely high snowfall rate ( $8\text{ mm h}^{-1}$ ) with a visibility-defined snowfall intensity of only moderate during a snowfall of heavily rimed crystals.

## 2) CASE 2: 29 MARCH 1995

Key feature—Unrimed dendrites showing good agreement with theory  
Temperature range— $-5.0^{\circ}$  to  $-7.5^{\circ}\text{C}$

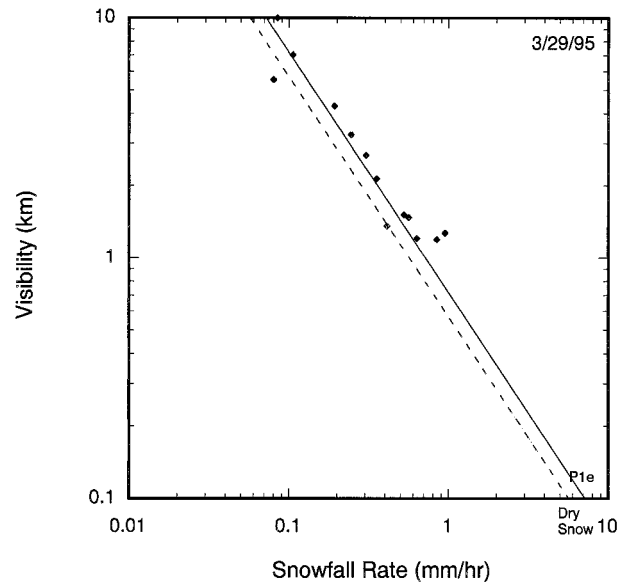


FIG. 17. Same as Fig. 16 but for 29 Mar 1995.

Range of wind speeds— $2.5$  to  $5.0\text{ m s}^{-1}$

Crystal types and size ranges—Dendrites (1–2 mm) and aggregates of dendrites

Degree of riming—None

Degree of aggregation and maximum aggregate size—Light, 10 mm

Range of snowflake terminal velocities—No data

Range of snowfall rates— $0$  to  $1\text{ mm h}^{-1}$

Snowfall started at 0700 UTC and continued at a light rate throughout the day. The temperature was  $-5^{\circ}\text{C}$  at 0700 UTC, cooled to  $-7.5^{\circ}\text{C}$  by 1200 UTC, and then heated back up to  $-5^{\circ}\text{C}$  by 0000 UTC next day. Crystal types were unrimed dendrites 1–2 mm in size, with a few aggregates up to 10 mm in diameter. Wind speed was less than  $5\text{ m s}^{-1}$  during the entire event. The data compare very favorably with the theoretical visibility–snowfall curve for dendrites (P1e; Fig. 17), showing relatively little scatter in the data.

## 3) CASE 3: 10 APRIL 1995

Key feature—Variety of crystal types leading to scatter in the visibility–snowfall rate relationship

Temperature range— $0.0^{\circ}$  to  $-7.5^{\circ}\text{C}$

Wind speed— $0.0$  to  $12.5\text{ m s}^{-1}$

Crystal types and size ranges—Sector plates, needles, rimed sector plates, rimed dendrites, and irregular crystals, 1–2 mm

Degree of riming—None to moderate

Degree of aggregation and maximum aggregate size—Light, 5 mm

Snowfall started at 0700 UTC following the passage of a cold front. Wind speeds during frontal passage were  $10$ – $12\text{ m s}^{-1}$ , dropping to  $5\text{ m s}^{-1}$  by 1100 UTC. The

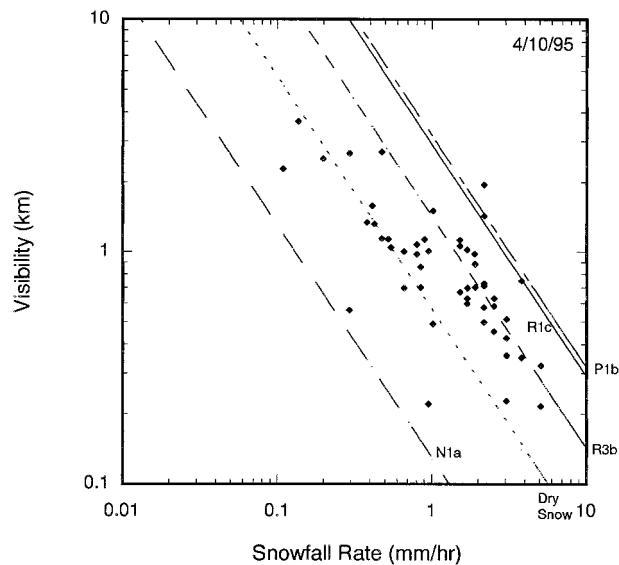


FIG. 18. Same as Fig. 16 but for 10 Apr 1995.

temperature at 0600 UTC was  $0^{\circ}\text{C}$ , dropping to  $-4^{\circ}\text{C}$  by 0800 UTC. The crystal types included sector plates (P1b), needles (N1a), rimed sector plates (R1c), rimed dendrites (R3b), and irregular crystals, with a mean size of 1 mm.

Comparison with the relevant visibility–snowfall curves (Fig. 18) shows that the data fall within the relevant crystal curves. Because of the wide range of crystals in this case, the data cover a large area of the plot. For instance, at a snowfall rate of  $2\text{ mm h}^{-1}$ , the visibility ranged from 0.2 km (heavy snow intensity) to nearly 2.0 km (light snow intensity). This variation is produced by mostly single, unrimed crystals of various types. Thus the variety of crystal types that occur during natural snowfalls can produce a wide degree of scatter in the visibility–snowfall relation. Note that the above result is for temperatures less than  $0^{\circ}\text{C}$ .

#### 4) CASE 4: 21 APRIL 1995

Key feature—Wet and rimed snowflakes leading to high visibility, high precipitation rate conditions

Temperature range— $-1.5^{\circ}$  to  $0.0^{\circ}\text{C}$

Range of wind speed— $0.0$  to  $2.5\text{ m s}^{-1}$

Crystal types and size ranges—Dendrites (1–5 mm)

Degree of riming—Light to moderate

Degree of aggregation and maximum aggregate size—Heavy (30 mm)

Range of snowfall rates— $0.1$  to  $8.0\text{ mm h}^{-1}$

Snowfall started at 1200 UTC and reached rates of up to  $8\text{ mm h}^{-1}$  shortly after 1300 UTC in association with large aggregates (nearly 30 mm in diameter) of dendrites at a temperature near  $0^{\circ}\text{C}$  and a terminal velocity of  $2\text{ m s}^{-1}$ . The visibility associated with this high snowfall period was 0.30 km, just barely into the heavy

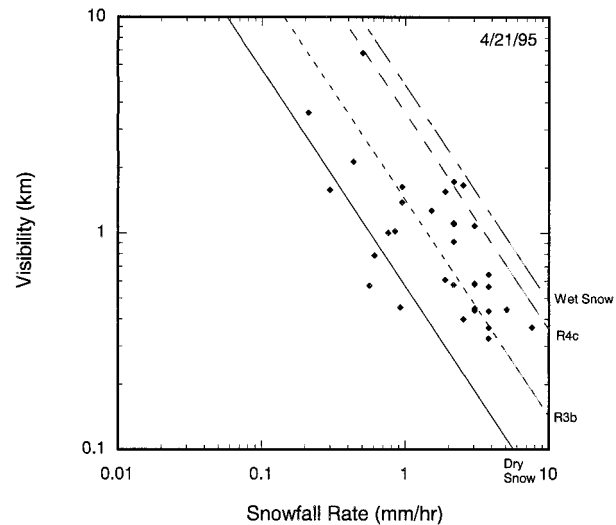


FIG. 19. Same as Fig. 16 but for 21 Apr 1995.

snow category. After 1400 UTC the snowfall rate decreased to values less than  $4\text{ mm h}^{-1}$  while the temperature increased to  $+0.5^{\circ}\text{C}$  and the degree of aggregation decreased and riming increased. By 1500 UTC the temperature increased to  $+1^{\circ}\text{C}$ , and the crystals became less aggregated and more heavily rimed (1–2 mm in size).

The wind speed during this entire snowfall period generally was very light at less than  $2.5\text{ m s}^{-1}$ . During the period between 1400 and 1530 UTC, snowfall rates ranged between 1 and  $4\text{ mm h}^{-1}$ , and visibilities ranged between 0.3 (heavy snowfall intensity) and 1.5 km (light snow intensity). This wide range in visibilities spans the theoretically predicted curves for densely rimed dendrites (R3b), graupel (R4c), and wet or rimed snow (Fig. 19), and results in high visibilities for snowfall rates near  $2\text{ mm h}^{-1}$  (up to 1.5 km). A few data points fall below the theoretical curves, suggesting that the dry snow in this case was of lower density than average. One of the unique aspects of this case was the presence of temperatures entirely warmer than  $0^{\circ}\text{C}$ , likely resulting in partial melting of the snowflakes and snow crystals, and the observed high terminal velocities of between 1.5 and  $2.0\text{ m s}^{-1}$  in agreement with the predicted terminal velocity of wet snowflake aggregates from Eq. (1). The melting process leads to a smaller crystal cross-sectional area from the soaking of melt-water into the interior of the crystal. Higher terminal velocities are also associated with rimed snowflakes and crystals as well (Table 2).

Most of the high visibility/high snowfall rate conditions occurred when the crystals were heavily rimed and not aggregated, although the early parts of the event also had relatively high visibilities for the extremely high snowfall rates observed (up to  $8\text{ mm h}^{-1}$ ) during a period of heavy aggregation (up to 30-mm diameter) and high terminal velocity ( $2\text{ m s}^{-1}$ ), suggesting that

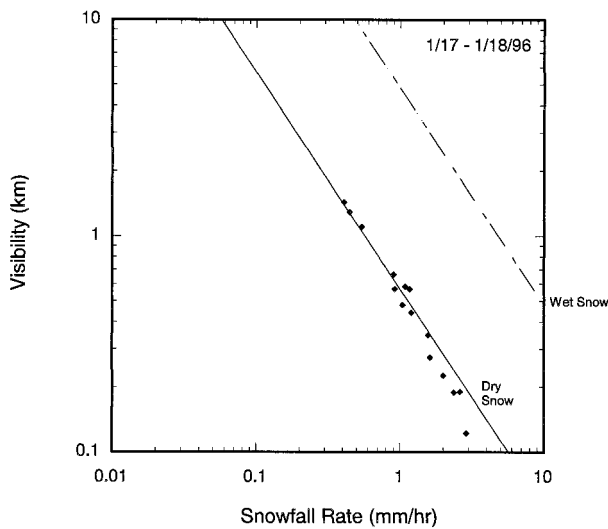


FIG. 20. Same as Fig. 16 but for 17–18 Jan 1996.

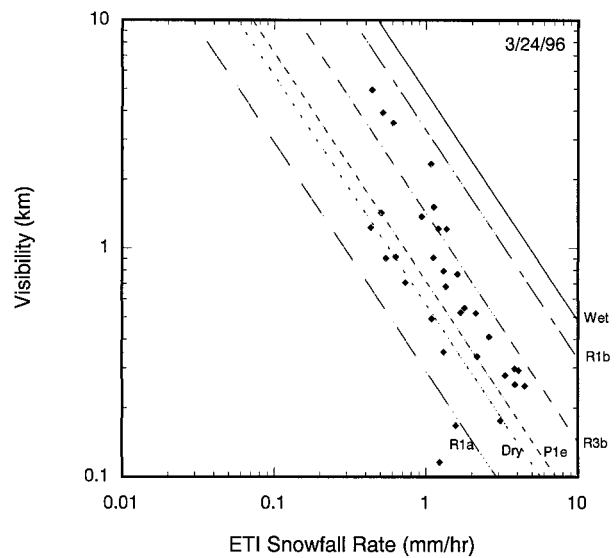


FIG. 21. Same as Fig. 16 but for 24 Mar 1996.

wet snowflakes also can lead to high visibilities during high snowfall periods, in agreement with theory.

#### 5) CASE 5: 17–18 JANUARY 1996

Key feature—Dry snowflakes showing good agreement with theory.

Temperature range— $-0.5^{\circ}$  to  $-15.0^{\circ}\text{C}$

Wind speed—2 to  $12\text{ m s}^{-1}$

Crystal types and size ranges—Aggregates of light to moderately rimed dendrites

Degree of riming—Light to moderate

Degree of aggregation and maximum aggregate size—Heavy (10 mm)

Range of terminal velocities— $1.0$  to  $1.2\text{ m s}^{-1}$

Range of snowfall rates— $0.3$  to  $3.0\text{ mm h}^{-1}$

The snow event was associated with the passage of an arctic front between 1700 and 1800 UTC, with temperatures decreasing from  $-0.5^{\circ}$  to  $-7^{\circ}\text{C}$  and wind speeds increasing from 2 to  $12\text{ m s}^{-1}$  during this period. Temperatures and wind speeds gradually decreased to  $-15^{\circ}\text{C}$  and  $3\text{ m s}^{-1}$ , respectively, by 0000 UTC 17 January.

Crystal types during this event were quite uniform and consisted of aggregates of light to moderately rimed dendrites, 5–10 mm in diameter, falling at a terminal velocity of  $1.0$ – $1.2\text{ m s}^{-1}$ . The comparison of the data with the dry snowfall theory [Fig. 20, Eq. (13)] shows excellent agreement. The good comparison with theory for this case in which the crystal type was very uniform over the entire event gives good support to both the theoretical approach and the observational data used in this study. It also suggests that visibility estimates of snowfall intensity are reasonable if the snow consists of dry snowflake aggregates.

#### 6) CASE 6: 24 MARCH 1996

Key feature—Variations in crystal type (needles to dendrites), degree of riming, and degree of aggregation, leading to scatter in the visibility–snowfall rate relationship

Temperature range— $0^{\circ}$  to  $-10^{\circ}\text{C}$

Range of wind speeds—2 to  $8\text{ m s}^{-1}$

Crystal types and size ranges—Light to heavily rimed dendrites, needles, and columns occasionally aggregated

Degree of riming—Light to heavy

Degree of aggregation and maximum aggregate size—Occasional, 10 mm

Range of terminal velocities— $0.7$  to  $1.5\text{ m s}^{-1}$

Range of snowfall rates— $0.3$  to  $4.0\text{ mm h}^{-1}$

This event was associated with a gradual frontal passage between 0000 and 1400 UTC, lowering temperatures from  $+2^{\circ}$  to  $-10^{\circ}\text{C}$ . Wind speeds were between 2 and  $8\text{ m s}^{-1}$ , and the snowfall rates were between 0.3 and  $4\text{ mm h}^{-1}$  during this period. As in many of the cases, snowfall rate was highest ( $\sim 4\text{ mm h}^{-1}$ ) at 0230 UTC just after the initial frontal passage. Snowfall started at 0130 UTC at a temperature of  $0^{\circ}\text{C}$ . Crystal types were moderate to heavily rimed dendrites (2–4-mm diameter), columns, and needles occasionally aggregated, with a few time periods with light rime. The comparison with theory (Fig. 21) shows a wide range of scatter that is consistent with the crystal types observed [moderately to heavily rimed dendrites (R3b), columns (R1b), and needles (R1a), and occasional presence of aggregates to 10-mm diameter]. In particular, note the large degree of scatter of the visibility data at a snowfall rate of  $1\text{ mm h}^{-1}$ , going from 0.1 (heavy snow intensity) to 2.2 km (light snow intensity). The low visibility measurement is consistent with heavily rimed needles (R1a), while

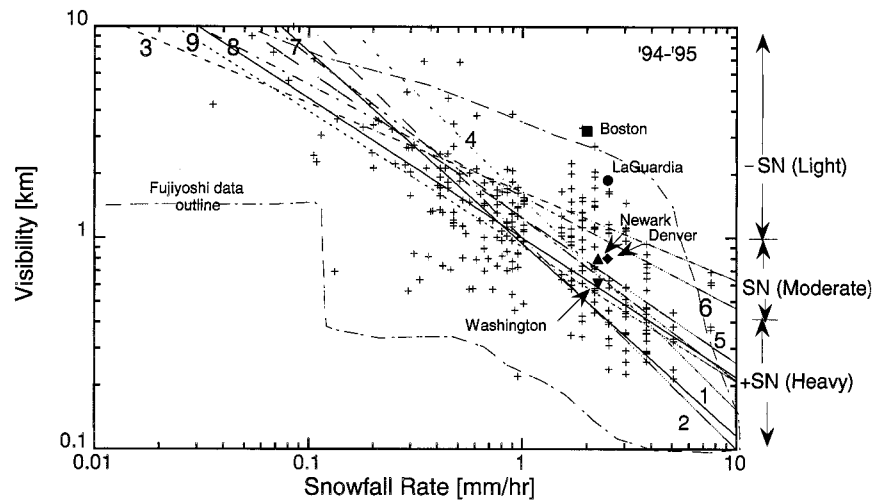


FIG. 22. Comparison of 1994/95 NCAR Marshall field site visibility and snowfall data (plus symbols) with previous visibility–snowfall rate correlations by Poljakova and Tretjakov (1960), curve 1 ( $V = 0.945S^{-0.91}$ ); Lillesaeter (1965), curve 2 ( $V = S^{-1}$ ); Mellor (1966), curve 3 ( $V = 1.65S^{-0.42}$ ); Warner and Gunn (1969), curve 4 ( $V = 1.54S^{-1}$ ); O'Brien (1970), curve 5 ( $V = 1.25S^{-0.69}$ ); Bisyarin et al. (1971), curve 6 ( $V = 1.57S^{-0.52}$ ); Muench and Brown (1977), curve 7 ( $V = 1.24S^{-0.77}$ ); Fujiyoshi et al. (1983), curve 8 ( $V = S^{-0.66}$ ); and Stallabrass (1985), curve 9 ( $V = 0.915S^{-0.64}$ ). Here  $V$  is visibility (in km) and  $S$  is liquid equivalent snowfall rate (in  $\text{mm h}^{-1}$ ). The dashed line is the outline of data scatter from Fujiyoshi et al. (1983). The bold symbols give the snowfall rate–visibility pairs for the various accidents listed in Table 1. The solid square is the Boston accident, solid circle is the La Guardia accident, solid diamond is the Denver accident, solid triangle pointing upward is the Newark accident, and solid triangle pointing downward is the Washington, District of Columbia, accident.

the high visibility value is consistent with heavily rimed dendrites (R3b) and heavily rimed columns (R1b), crystal types observed during this storm. Again, the observed scatter likely is caused by the variation in crystal type from needles to columns to dendrites, the degree of riming, and the absence or presence of aggregation during various time periods of this storm. Under rapidly changing conditions, visibility is an unreliable indicator of snowfall intensity unless crystal types and degree of riming and aggregation are known in real time.

#### b. Comparison with previous observations

Previous studies of the relationship between snowfall rate and visibility (Fujiyoshi et al. 1983; Mellor 1966; Lillesaeter 1965; Bisyarin et al. 1971; Muench and Brown 1977; O'Brien 1970; Poljakova and Tretjakov 1960; Robertson 1973; Stallabrass 1985; Warner and Gunn 1969) are compared with the current observations in Fig. 22 (1994/95 results) and Fig. 23 (1995/96 results).

The curves from previous studies of the relationship between snowfall rate and visibility also show a large degree of scatter, especially at the higher snowfall rates. For instance, at a snowfall rate of  $2.5 \text{ mm h}^{-1}$ , the visibility ranges from 0.35 (heavy snow based on visibility criteria) to 2.3 km (light snow based on visibility criteria), similar to the theoretical scatter in Fig. 8. The above variation is for the best-fit curves to the data from

the respective investigators. The actual data scatter in these previous studies is very similar to the scatter obtained in the current study (plotted as the plus signs in Figs. 22 and 23). For comparison, data from Fujiyoshi et al. (1983) for snowstorms in Japan are reproduced as the dashed outline. The scatter in the Fujiyoshi et al. (1983) data is very similar to the scatter observed in the current results. They also attributed the large degree of scatter to the variety of crystal types observed, and suggested that one may be able to determine the crystal type by the observed Vis– $S$  relationship. The current theoretical results support this suggestion. A number of studies (Lillesaeter 1965; Robertson 1973; Warner and Gunn 1969) also found higher visibilities during wet or rimed snow conditions, consistent with the current results. Higher correlations also were found for individual crystal types than for the sample as a whole by Stallabrass (1985), O'Brien (1970), and Fujiyoshi et al. (1983), in agreement with the findings of this study.

Thus, both the current and previous results show that there is a large degree of scatter in Vis– $S$  relationships as a result of the natural variability of snow crystal types, degree of riming, degrees of aggregation, and degrees of crystal wetness.

The bold symbols in Figs. 22 and 23 are the visibility and snowfall rate conditions associated with the ground-icing accidents listed in Table 1. Note that the variation in visibility (and consequently snow intensity as indicated by the scale on the right-hand side of the fig-

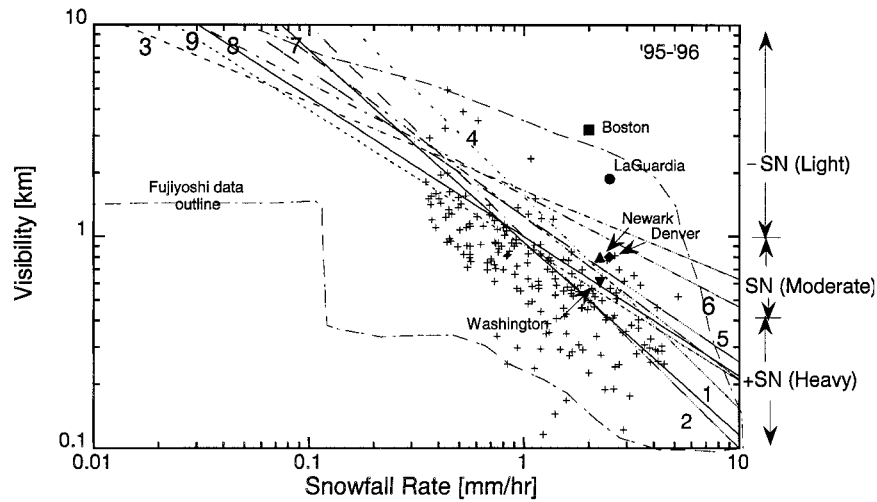


FIG. 23. Same as Fig. 22 but for NCAR Marshall field site snowfall and visibility from the winter of 1995/96.

ures) for the nearly constant snowfall rates observed during the accidents spans the same range as the current and previous data do and also spans the light to moderate snow intensity categories. Thus, the use of visibility to estimate snowfall rate clearly can be misleading in many cases and may have been a factor in these accidents.

## 6. Effect of nightfall on the estimation of snowfall by visibility

Visibility is defined generally as that distance at which human vision can just detect the presence of an object from the background. The physical and physiological mechanisms used to perform this detection are different during the day and at night. At night the determination of visibility usually is done with low-wattage nondirectional lights, while during the day objects are compared to the background luminance to determine visibility. Both determinations are done with the unaided human eye. Automatic visibility measurements using instruments can duplicate this human observation reasonably if different algorithms are applied during the day and during the night. In the following, the method and equations used to determine visibility during the day and night are briefly described separately, and then the effect that the differences between these two approaches have on the estimation of snowfall rate using visibility is discussed. The discussion in sections 6a and 6b below follow the presentation by Lenschow (1986). For further information on day and night visibility measurements and theory, see Douglas and Booker (1977).

### a. Daytime visibility

The farther an object is from an observer, the greater its apparent luminance becomes, until at some distance it becomes indistinguishable from the background lu-

minance. This distance is defined as the daytime visibility and is sensitive to the visual contrast threshold of the observer's eye and to the background luminance. The apparent "lightening" of the object is caused by the scattering of sunlight by atmospheric particles, hydrometeors, and gases between the observer and the object being observed and by sunlight being diffusely reflected from the ground into the eye of the observer. If a black object is considered, then the following equation for the apparent contrast  $C$  between the object and the background at a distance  $R$  from the observer can be written (Middleton 1954):

$$C = |(B'_o - B'_h)/B_h| = \exp(-\sigma R), \quad (20)$$

where  $B'_o$  is the brightness of the object at the location of the observer a distance  $R$  from the object,  $B'_h$  is the brightness of the background at a distance  $R$  from the object, and  $\sigma$  is the atmospheric extinction coefficient averaged over the distance  $R$  and over the visible spectrum.

If an observer moves away from a black object with the horizon sky behind it,  $C$  decreases according to the above equation until at some distance  $R$  it becomes equal to the visual contrast threshold  $\epsilon$ . This distance  $R$  is defined as the daytime visibility  $V_d$  and is given by (Middleton 1954)

$$\epsilon = \exp(-\sigma V_d). \quad (21)$$

This equation assumes that the background brightness is constant with distance from the observer. The contrast threshold  $\epsilon$  of the observer's eye usually is assumed to be constant at 0.02 or 0.055, although in some cases it can be much less with nonblack objects. Its precise value depends on various factors of luminance and the object angle subtended by the eye at the target distance  $R$ . This equation originally was derived by Koschmieder (1924) and has been used successfully to estimate visibility

during daytime conditions. Equation (3) in section 2a can be derived from Eq. (21) by setting  $\epsilon = 0.02$ .

*b. Nighttime visibility*

Nighttime visibility is defined as the horizontal distance at which a point source of light of luminous intensity  $I_o$  is just visible by the human eye. The illuminance  $E$  at a distance  $R$  from a source of light of intensity  $I_o$  in a medium of path-averaged extinction coefficient  $\sigma$  is given by Allard's law as

$$E = \frac{I_o \exp(-\sigma R)}{R^2}. \tag{22}$$

This equation shows that the illuminance of a point source of light falls off as the radius squared, and also decreases exponentially with distance from the light source through scattering and absorption by particles and gases in the medium.

The human eye can only detect light above a certain threshold illuminance  $E_t$ . Threshold illuminance  $E_t$  is not a constant but is a function of the background luminance, the position of the light in the field of view, the angular size and shape of the light, and its color and distance from the observer. If the background luminance is higher (such as nearer a city), then the threshold illuminance also is higher, in order for the observer to detect the difference between the background and the light source. If the light source varies, this variation also will affect the estimate of visibility. To take into account the variations in the threshold illuminance  $E_t$  with distance, Douglas and Booker (1977) used the following relation:

$$E_t = \frac{C_{DB}}{V_n}, \tag{23}$$

where  $C_{DB}$  is a constant of proportionality and  $V_n$  is the nighttime visibility.

Substituting the above equation into Eq. (22) yields a simplified Allard's law:

$$V_n = \frac{I_o}{C_{DB}} \exp(-\sigma V_n). \tag{24}$$

*c. Comparison between nighttime and daytime visibility and its effect on the estimation of snowfall intensity*

The U.S. National Weather Service visibility algorithm for its ASOS systems uses Koschmieder's Eq. (21) with  $\epsilon = 0.055$  to estimate day visibility, and the simplified Allard's law [(24)] with  $I_o = 25$  candles and  $C_{DB} = 0.084 \text{ mi}^{-1}$  to estimate night visibility. Since two different techniques are used during daytime and nighttime, it is of interest to compare the visibility estimated during these two periods for the same extinction coefficient. If Koschmieder's law [(21)] and the simplified Allard's law [(24)] are combined by eliminating  $\sigma$ , one

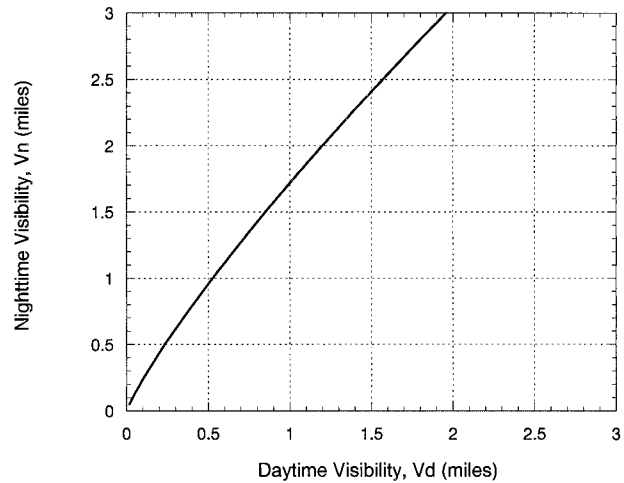


FIG. 24. Nighttime visibility vs daytime visibility for the same extinction coefficient  $\sigma$  using the ASOS parameters for  $I_o$ ,  $\epsilon$ , and  $C_{DB}$  ( $I_o = 25$  candles,  $\epsilon = 0.055$ , and  $C_{DB} = 0.084 \text{ mi}^{-1}$ ).

can write the following equation showing the relationship between  $V_n$  and daytime visibility  $V_d$ :

$$V_d = \frac{\ln(\epsilon)V_n}{\ln(C_{DB}V_n/I_o)}. \tag{25}$$

Figure 24 shows the relationship between night and day visibility using Eq. (25) with  $\epsilon = 0.055$ ,  $I_o = 25$  candles,  $C_{DB} = 0.084 \text{ mi}^{-1}$  (ASOS parameters), and visibility in miles. When the visibility is low (less than 0.1 mi in the daytime), a 25-candle light can be seen at night more than 2.4 times as far as a large black object would be seen at the same distance during the daytime. For a daytime visibility of 0.5 mi, the same black object can be seen a little less than twice as far at night as during the day. This difference decreases as the visibility increases, becoming about equal when the object is 15 mi away.

In regard to the estimation of snowfall intensity using visibility, the current National Weather Service definition states that heavy snow intensity occurs when the visibility is less than or equal to 1/4 mi, moderate intensity when the visibility is between 5/16 and 5/8 mi, and light intensity for visibilities greater than 5/8 mi. Referring to Fig. 24, these visibility ranges for daytime would result in a factor of 2 higher visibility during the night. Thus, reported snowfall intensities would be expected to be one category less intense during the night than during the day because of the different method of determining visibility at night, if the snowfall conditions remain the same (extinction coefficient does not change). This phenomenon would pertain to a human observer using 25-candle lights to determine visibility and to any automatic system such as ASOS that uses Allard's law to estimate nighttime visibility.

Thus, visibility-based estimates of snow intensity at night by either an observer or by the ASOS using Koschmieder's law during the day and Allard's law at

TABLE 6. Modified visibility criteria for snow intensity based on temperature and day vs night (visibility as reported by ASOS in statute miles).

Condition/temperature	Snow intensity			
	Heavy	Moderate	Light	
Daytime	< -1°C	¼	½	≥¾
	≥ -1°C	≤½	¾	≥1
Nighttime	< -1°C	≤½	¾	≥1
	≥ -1°C	≤¾	1 to 1.25	>1.25

night should be increased by one category in order not to underestimate the snow intensity, because of the inherently better visibility at night than during the day. During the night, light snow intensity based on visibility should be increased to moderate, and moderate snow intensity should be increased to heavy, as shown in Table 6. Also shown in this table is a suggested adjustment of snowfall intensity using visibility and temperature to account for the more frequent occurrence of wet snow and riming at warmer temperatures.

## 7. Conclusions

The previous sections have shown from both observations and theory that a given visibility is not uniquely related to only one liquid equivalent snowfall rate because of the variety of crystal types, degrees of riming, degrees of aggregation, degrees of crystal wetness, and the difference from day to night in determining visibility. A unique relationship for a given storm occurred only when the crystal types did not vary significantly in time. For instance, the heavily aggregated dry snowfall on 17 January 1996 (Fig. 20) showed an excellent relationship between visibility and liquid equivalent snowfall rate that lasted the entire event. Storms with single crystal types were the exception in the 2-yr dataset, however, and most storms had a variety of crystal types and degrees of riming, aggregation, and wetness during various stages of the storm. As a result, the current operational method to estimate snowfall intensity by visibility should only be used as a guideline for snowfall intensity and not as a reliable source for liquid equivalent snowfall rates, especially during wet snow, snowfall with significant amounts of riming or single crystals of compact shape, and during the night. For instance, a moderate snowfall rate (estimated in the current study to be between 1 and 2.5 mm h<sup>-1</sup>) can occur for visibilities between 0.3 and 2.0 km, while a heavy snowfall rate (>2.5 mm h<sup>-1</sup>) can occur between visibilities of 0.2 and 0.8 km, for temperatures less than 0°C.

During the night the visibility determined by an observer or ASOS will increase by a factor of 2 over the daytime visibility for the same liquid equivalent snowfall rate, resulting in heavy snowfall intensity being converted to moderate, and moderate snowfall intensity being converted to light.

The above results suggest that the light snow intensities and high visibilities reported during the La Guardia accident despite the relatively high liquid equivalent snowfall rate observed (see Table 1 and Figs. 22 and 23), likely can be explained in terms of the presence of wet or rimed snow consisting of small flakes (as reported by the National Weather Service observer and the second officer of the flight) and the increase in reported visibility due to its occurrence at night.

To avoid these uncertainties associated with the estimation of snowfall rate by visibility, future airport and other weather systems should measure the liquid equivalent snowfall rate directly using snow gauges or other such devices. The ASOS program currently is evaluating a number of weighing-type snow gauges for inclusion in the currently deployed ASOS system. New weather systems, such as the Weather Support to Deicing Decision Making system (Rasmussen et al. 1999) provide real-time estimates of liquid equivalent snowfall rates to airlines and airports using snow gauges. These direct methods of measuring snowfall rate are strongly recommended over indirect methods such as visibility.

*Acknowledgments.* We would like to thank Rachel Ames and Eli Karplus for their assistance in processing the data presented in this report, and Carol Makowski for typing and editing this manuscript. This work also benefited from extensive discussions with Chuck Wade regarding the accuracy of snow gauges to estimate snow accumulation. The authors also appreciate the constructive comments of three anonymous reviewers. This work was supported under contracts from the William J. Hughes FAA Technical Center, Transport Canada, and the FAA Aviation Weather Research Program. This research is in response to requirements and funding by the Federal Aviation Administration. The views expressed are those of the authors and do not necessarily represent the official policy of the U.S. government.

## REFERENCES

- Bisyrin, V. P., I. P. Bisyarina, V. K. Rubash, and A. K. Sokolov, 1971: Attenuation of 10.6 and 0.63  $\mu\text{m}$  laser radiation in atmospheric precipitation. *Radio Eng. Electron. Phys.*, **16**, 1594–1597.
- Braham, R. R., 1990: Snow particle size spectra in lake effect snow. *J. Appl. Meteor.*, **29**, 200–207.
- Conway, J. H., and N. J. A. Sloane, 1993: *Sphere Packings, Lattices and Groups*. Springer-Verlag, 744 pp.
- Davis, C. I., 1974: The ice nucleating characteristics of various AgI aerosols. Ph.D. thesis, University of Wyoming, 135 pp. [Available from University of Wyoming, Box 3108, Laramie, WY 82071-3334.]
- Douglas, C. A., and R. L. Booker, 1977: *Visual Range: Concepts, Instrumental Determination, and Aviation Applications*. NBS Monogr., No. 159, Department of Commerce, 362 pp.
- Fujiyoshi, Y., G. Wakahamam, T. Endoh, S. Irikawa, H. Konishi, and M. Takeuchi, 1983: Simultaneous observation of snowfall intensity and visibility in winter at Saporro. *Low Temp. Sci.*, **42A**, 147–156.

- Heymsfield, A. J., 1972: Ice crystal terminal velocities. *J. Atmos. Sci.*, **29**, 1348–1357.
- , and M. Kajikawa, 1987: An improved approach to calculating terminal velocities of plate-like crystals and graupel. *J. Atmos. Sci.*, **44**, 1088–1099.
- Holroyd, E. W., III, 1971: The meso- and microscale structure of Great Lakes snowstorm bands—A synthesis of ground measurements, radar data, and satellite observations. Ph.D. dissertation, State University of New York at Albany, 148 pp. [Available from State University of New York at Albany, 1400 Washington Ave., Albany, NY 12222.]
- Houze, R. A., Jr., P. V. Hobbs, P. H. Herzegh, and D. B. Parsons, 1979: Size distributions of precipitation particles in frontal clouds. *J. Atmos. Sci.*, **36**, 156–162.
- Iwai, K., 1973: On the characteristic features of snow crystals developed along c-axis. *J. Meteor. Soc. Japan*, **51**, 458–465.
- Jayaweera, K. O. L. F., and B. J. Mason, 1965: The behaviour of freely falling cylinders and cones in a viscous fluid. *J. Fluid Mech.*, **22**, 709–720.
- , and R. E. Cottis, 1969: Fall velocities of plate-like and columnar ice crystals. *Quart. J. Roy. Meteor. Soc.*, **95**, 703–709.
- , and T. Ohtake, 1974: Properties of columnar ice crystals precipitating from layer clouds. *J. Atmos. Sci.*, **31**, 280–286.
- Koschmieder, H., 1924: Theorie der horizontalen Sechsteite (Theory of horizontal visibility). *Beitr. Phys. freien Atmos.*, **12**, 33–53, 171–181.
- Lenschow, D., 1986: *Probing the Atmospheric Boundary Layer*. Amer. Meteor. Soc., 269 pp.
- Lillesaeter, O., 1965: Parallel-beam attenuation of light, particularly by falling snow. *J. Appl. Meteor.*, **4**, 607–613.
- Magono, C., and T. Nakamura, 1965: Aerodynamic studies of falling snowflakes. *J. Meteor. Soc. Japan*, **43**, 139–147.
- Mellor, M., 1966: Light scattering and particle aggregation in snow storms. *J. Glaciol.*, **6**, 607–613.
- Middleton, W. E. K., 1954: *Vision through the Atmosphere*. University of Toronto Press, 250 pp.
- Mitchell, D. L., R. Zhang, and R. L. Pitter, 1990: Mass-dimensional relationships for ice particles and the influence of riming on snowfall rates. *J. Appl. Meteor.*, **29**, 153–163.
- Muench, H. S., and H. A. Brown, 1977: Measurements of visibility and radar reflectivity during snowstorms in the AFGL mesonet. Environmental Res. Paper AFGL-TR-77-0148, 36 pp. [Available from the Meteorology Division, Project 8628, Air Force Geophysics Laboratory, Hanscom AFB, MA 01731.]
- National Weather Service, 1994: Surface observations. *Observing Handbook 7*, U.S. Department of Commerce, 186 pp. [Available from NOAA, National Weather Service, Office of Systems Operations, Observing Systems Branch, 1325 East-West Highway, Silver Spring, MD 20910.]
- O'Brien, H. W., 1970: Visibility and light attenuation in falling snow. *J. Appl. Meteor.*, **9**, 671–683.
- Ono, A., 1969: The shape and riming properties of ice crystals in natural clouds. *J. Atmos. Sci.*, **26**, 138–147.
- Poljakova, E. A., and V. D. Tretjakov, 1960: Visibility in falling snow. *Glav. Geofiz. Obs.*, **100**, 53–57.
- Press, W. H., B. P. Flannery, S. A. Teukowsky, and W. T. Vetterling, 1986: *Numerical Recipes*. Cambridge University Press, 818 pp.
- Pruppacher, H. R., and J. D. Klett, 1997: *Microphysics of Clouds and Precipitation*. Kluwer Academic, 954 pp.
- Rasmussen, R. M., J. Cole, and K. Knight, 1995: Meteorological conditions associated with ground de-icing accidents and the effects of wind on snowfall accumulation on aircraft. Preprints, *Sixth Conf. on Aviation Weather Systems*, Dallas, TX, Amer. Meteor. Soc., 261–265.
- , and Coauthors, 1999: Weather Support to Deicing Decision Making (WSDDM): A winter weather nowcasting system. Preprints, *Eighth Conf. on Aviation, Range, and Aerospace Meteorology*, Dallas, TX, Amer. Meteor. Soc., 462–466.
- Robertson, C. E., 1973: The reliability of an optical technique for measuring snowfall rates. *J. Appl. Meteor.*, **12**, 553–555.
- Rogers, D. C., 1974: The aggregation of natural ice crystals. Rep. AR110, 91 pp. [Available from Department of Atmospheric Resources, College of Engineering, University of Wyoming, Laramie, WY 82072.]
- Schmidt, R. M., 1981: Estimates of threshold windspeed from particle sizes in blowing snow. *Cold Reg. Sci. Technol.*, **4**, 187–197.
- Stallabrass, J. R., 1985: Measurements of the concentration of falling snow. Tech. Memo. 140, *Snow Property Measurements Workshop*, Lake Louise, AB, Canada, National Research Council Canada, 20 pp.
- Tabler, R. D., 1984: Using visual range data for highway operations in blowing snow. *Opt. Eng.*, **23**, 55–61.
- Warner, C., and K. L. S. Gunn, 1969: Measurement of snowfall by optical attenuation. *J. Appl. Meteor.*, **8**, 110–121.
- Willmarth, W. W., N. E. Hawk, and R. L. Harvey, 1964: Steady and unsteady motions and wakes of freely falling disks. *Phys. Fluids*, **7**, 197–208.
- Zikmunda, J., and G. Vali, 1972: Fall patterns and fall velocities of rimed ice crystals. *J. Atmos. Sci.*, **29**, 1334–1347.